Citrullination of HP1γ chromodomain affects association to chromatin

Meike Wiese[1,2*], Andrew J. Bannister[1,2], Srinjan Basu[3#], Wayne Boucher[3], Kai Wohlfahrt[3], Maria A. Christophorou[4], Michael L. Nielsen[5], David Klenerman[6], Ernest D. Laue[3], Tony Kouzarides[1,2#]

[1]The Gurdon Institute, University of Cambridge, Tennis Court Road, Cambridge, CB2 1QN, United Kingdom.
[2]Department of Pathology, University of Cambridge, Tennis Court Road, Cambridge, CB2 1QP, United Kingdom.
[3]Department of Biochemistry, University of Cambridge, 80 Tennis Court Road, Cambridge, CB2 1GA, United Kingdom.
[4]Institute of Genetics and Molecular Medicine, University of Edinburgh, Western General Hospital, Crewe Road South, Edinburgh, EH4 2XU, United Kingdom.
[5]Department of Proteomics, The Novo Nordisk Foundation Center for Protein Research, University of Copenhagen, Faculty of Health Sciences, Blegdamsvej 3b, DK-2200 Copenhagen, Denmark.
[6]Department of Chemistry, University of Cambridge, Lensfield Road, Cambridge, CB2 1EW, United Kingdom

#: corresponding authors; *: first author

Authors' email addresses:

Dr. Meike Wiese:	wiese@ie-freiburg.mpg.de
Dr. Andrew J. Bannister:	ab149@cam.ac.uk
Dr. Srinjan Basu:	sb451@cam.ac.uk
Dr. Wayne Boucher:	wb104@cam.ac.uk
Dr. Kai Wohlfahrt:	Kai.wohlfahrt@gmail.com
Dr. Maria A. Christophorou:	maria.christophorou@igmm.ed.ac.uk
Prof. Michael L. Nielsen:	michael.lund.nielsen@cpr.ku.dk
Prof. David Klenerman:	dk10012@cam.ac.uk
Prof. Ernest Laue:	e.d.laue@bioc.cam.ac.uk
Prof. Tony Kouzarides:	t.kouzarides@gurdon.cam.ac.uk

Keywords: Chromatin, citrullination, stem cell differentiation

Abstract

Background

Stem cell differentiation involves major chromatin reorganization, heterochromatin formation and genomic relocalization of structural proteins, including heterochromatin protein 1 gamma (HP1γ). As the principal reader of the repressive histone marks H3K9me2/3, HP1 plays a key role in numerous processes including heterochromatin formation and maintenance.

Results

We find that HP1γ is citrullinated in mouse embryonic stem cells (mESCs) and this diminishes when cells differentiate, indicating that it is a dynamically regulated post-translational modification during stem cell differentiation. Peptidylarginine deiminase 4 (PADI4), a known regulator of pluripotency, citrullinates HP1γ *in vitro.* This requires R38 and R39 within the HP1γ chromodomain and the catalytic activity is enhanced by trimethylated H3K9 (H3K9me3) peptides. Mutation of R38 and R39, designed to mimic citrullination, affects HP1γ binding to H3K9me3-containing peptides. Using live-cell single-particle tracking, we demonstrate that R38 and R39 are important for HP1γ binding to chromatin *in vivo.* Furthermore, their mutation reduces the residence time of HP1γ on chromatin in differentiating mESCs.

Conclusion

Citrullination is a novel post-translational modification of the structural heterochromatin protein HP1γ in mESCs, that is dynamically regulated during

mESC differentiation. The citrullinated residues lie within the HP1γ chromodomain and are important for H3K9me3 binding *in vitro* and chromatin association *in vivo*.

Introduction

Embryonic stem cells (ESCs) are pluripotent cells with the unique ability to self-renew and differentiate into nearly every cell type of the body. This plasticity is maintained by a distinct nuclear architecture with particular epigenetic signatures including enrichment of active chromatin marks and dynamic binding of structural chromatin proteins (1, 2).

HP1 was originally described as a dominant suppressor of position-effect variegation in *Drosophila melanogaster* (3). The mammalian HP1 protein family consists of three members: HP1α, β and γ. As the main reader of repressive histone marks H3K9me2/3, HP1 is a key factor in heterochromatin formation and maintenance (4, 5). However, whilst HP1α and β are mainly associated with constitutive heterochromatic regions, HP1γ is predominantly found in euchromatin (6, 7), within the transcribed regions of active genes. Here, it regulates transcriptional elongation (8-11) and co-transcriptional mRNA processing (7, 12).

HP1γ plays important roles in developmental processes and cell fate decisions (13). For instance, depletion of HP1γ in mESCs results in endodermal and neuronal differentiation defects (14, 15). Interestingly, HP1γ is differentially localised during mESC differentiation. In mESCs, it

predominantly occupies gene bodies, whereas in neuronal precursor cells (NPCs), it is significantly enriched at the promoters of active genes (14, 16). This indicates a direct role for HP1γ regulating transcription during differentiation. However, little is known concerning how the recruitment of HP1γ and its association to specific genomic loci is regulated.

Peptidyl citrullination (deimination) is the post-translational conversion of an arginine (R) residue within a protein to the non-encoded amino acid citrulline. This leads to loss of a positive charge and a reduction in hydrogen bonding ability. It is mediated by a vertebrate-specific family of enzymes called peptidylarginine deiminases (PADIs) which are associated with the development of different pathological conditions such as autoimmunity, cancer and neurodegenerative diseases (17). The deiminases are widely expressed in mammalian tissues and PADIs 1, 2 and 4 have been reported to localise to the nucleus (18-20). Histones are the best-characterised nuclear targets of PADI enzymes and their citrullination is directly linked to transcriptional regulation (18-22).

We previously identified a role for PADI4 during reprogramming and ground state pluripotent stem cells (22), where the deiminase regulates key-pluripotency genes via a mechanism involving citrullination of H1.2. This results in its eviction from chromatin and global chromatin decompaction. Here, we report that the chromodomain of HP1γ is also citrullinated in mESCs, at R38 and R39. We show that binding of HP1γ to peptides bearing H3K9me3 enhances its citrullination by PADI4 *in vitro.* Furthermore, mutations

110 in HP1γ designed to mimic the loss of charge caused by citrullination inhibit
111 binding of HP1γ to peptides harboring H3K9me3, and reduce its residence
112 time on chromatin in differentiating mESCs. We also observe a reduction in
113 the level of HP1γ citrullination upon mESC differentiation. These results
114 support a role for citrullination as a mechanism to regulate HP1γ chromatin
115 association during stem cell differentiation.
116

117 Results

118 *HP1γ chromodomain is citrullinated in vivo*

119 We previously used tandem mass spectroscopy (MS/MS) to identify
120 citrullinated proteins in mESCs (22). We have now performed a more
121 thorough interrogation of these data using an improved search algorithm to
122 identify additional citrullinated chromatin associated proteins (Christophorou
123 *et al*., manuscript in preparation). This analysis detected two citrullinated sites
124 within the chromodomain of HP1γ (Fig 1A, Sup Fig 1A). More specifically, the
125 presence of immonium ions unique for citrulline (referred to as Im/(Cit) at m/z
126 130) and arginine (referred to as Im/(Arg) at m/z 129) were detected in two
127 peptides (Fig 1B and C). This strongly implies the presence of both citrulline
128 and arginine in these peptides. In the first peptide, citrullination of R38 was
129 identified with a localization probability of 0.71 (Fig 1B, Sup Fig 1B). MS/MS
130 analysis of the second peptide identified citrullination at either R38 or R39,
131 each with a localization score of 0.50 (Fig 1C, Sup Fig 1C). Taken together,
132 our MS data indicate that HP1γ is citrullinated in mESCs at either R38 or R39,
133 most likely the former. However, it is possible that both R38 and R39 are
134 citrullinated.

135

136 ***Loss of charge at R38 and R39 impairs HP1γ binding to H3K9me3***

137 Citrullination of arginine neutralizes the charge of the side-chain. Given that
138 R38 and R39 are located within the chromodomain of HP1γ, we investigated
139 whether they are important for binding H3K9me3. We generated recombinant
140 full-length mouse HP1γ proteins, either wild type (WT) or with alanine
141 substitutions at amino acids 38 and 39 to mimic citrullination (Sup Fig 1D). *In*
142 *vitro* peptide pulldown assays were used to test the binding of HP1γ to
143 unmethylated H3(1-16) or methylated H3K9me3(1-16) peptides. As expected,
144 HP1γ specifically binds to H3K9me3 peptides (Fig 2A, Sup Fig 2A). In
145 contrast, we observed that binding of double alanine mutant HP1γR38/9A to
146 H3K9me3 peptides was significantly reduced (Fig 2A, Sup Fig 2A).

147

148 We confirmed these results by assessing real-time binding kinetics of GST-
149 HP1γ proteins to immobilized H3 or H3K9me3 peptides using bio-layer
150 interferometry (BLI). As expected, HP1γWT binds exclusively to H3K9me3
151 peptides (Fig 2B, Sup Fig 2B and C, Table 1), which agrees with previously
152 published analyses (23). We repeated these analyses at a range of different
153 GST-protein concentrations (Sup Fig 2C). Again, the HP1γR38/9A mutant
154 protein displayed a distinctly different kinetic behaviour compared to the WT
155 protein (Fig 2B, Sup Fig 2B and C, Table 1). Binding of HP1γR38/9A appears
156 to begin to plateau at significantly lower amounts compared to the WT protein.
157 These results confirm the data obtained from pulldown assays (Fig 2A, Sup
158 Fig 2A). However, a more thorough biophysical analysis is required to fully

159 assess the kinetic behaviour of HP1γR38/9A molecules binding to H3K9me3
160 sites.
161
162 Interestingly, mutation of both R38 and R39 to lysine (R38/9K), which retains
163 the positive charge at these positions, maintained binding to H3K9me3
164 peptides in pulldown assays (Sup Fig 2A), as well as in BLI measurements
165 (Sup Fig 2B and C, Table 1). These results suggest that positive charges at
166 amino acids R38 and R39 are required for efficient HP1γ binding to H3K9me3
167 peptides.
168
169 ***PADI4 citrullinates HP1γ in vitro***
170 PADI4 is nuclear in mESCs and previous studies from our laboratory, as well
171 as others, identified several chromatin-associated (histone and non-histone)
172 substrates of the deiminase (21, 22, 24, 25). Therefore, we next asked
173 whether recombinant purified PADI4 citrullinates HP1γ in *in vitro* citrullination
174 assays. Enzymatic activity of recombinant PADI4 was confirmed by
175 citrullination of histone H3 - a known substrate of PADI4 (18) (Sup Fig 3A and
176 B). Using an anti-peptidyl-citrulline antibody, we found that PADI4 citrullinates
177 HP1γ *in vitro* (Fig 3A, Sup Fig 3C). To determine whether PADI4 citrullinates
178 HP1γ at positions 38 and 39, we substituted amino acid R38 and/or R39 with
179 lysine. Citrullination of HP1γ was abolished in both R38K and R39K mutant
180 proteins (Fig 3A, Sup Fig 3C), indicating that (i) both arginines are required for
181 PADI4 to target HP1γ, and (ii) R38 and/or R39 are citrullinated by PADI4 *in*
182 *vitro*.
183

184 Interestingly, addition of methylated H3K9me3 peptides to the *in vitro*
185 citrullination assay increased HP1γ citrullination by PADI4 by approximately 2-
186 fold (Fig 3B, Sup Fig 3D). The enhanced citrullination appears specific
187 because it was abolished when the HP1γR38/9K mutant protein was used as
188 a substrate (Fig 3B, Sup Fig 3D), even though this protein binds H3K9me3
189 peptides with similar affinity to the WT protein (Sup Fig 2). We conclude that
190 PADI4 preferentially citrullinates HP1γ at R38 and R39 when the protein is
191 bound to H3K9me3 peptides.
192
193 ***HP1γ citrullination is reduced in differentiating mESCs***
194 Our data indicate that citrullination occurs in HP1γ at R38 and R39 (Fig 1, Fig
195 3). We next inquired whether citrullination of R38 and R39 could be
196 differentially regulated *in vivo*. Citrullination of H1.2 by PADI4 during
197 reprogramming of mouse embryonic fibroblasts (MEFs) highlights a role for
198 citrullination in regulating stem cell plasticity (22). Furthermore, both PADI4
199 and HP1γ are involved in regulating the integrity of pluripotent stem cells (16,
200 22). We therefore assessed whether citrullination of HP1γ decreases upon
201 stem cell differentiation, as would be expected given the decrease in *PADI4*
202 gene expression during this process [22]. We induced differentiation in
203 mESCs cultured under serum/LIF by LIF withdrawal for 72h (Fig 4A). After 72
204 hours, the mRNA levels of the pluripotency markers *Nanog*, *Klf4* and *Oct4*
205 were down-regulated (Fig 4B) which was accompanied by clear morphological
206 changes (Fig 4C), indicating that mESCs were beginning to differentiate. We
207 then immunoprecipitated HP1γ from nuclear lysates of mESCs cultured with
208 or without LIF. Immunoblotting of the extracts using an anti-peptidyl-citrulline

209 antibody showed that HP1γ is indeed significantly less citrullinated in
210 differentiating mESCs (Fig 4D, Sup Fig 4A). This finding not only validates the
211 identification of HP1γ citrullination in our MS analysis (Fig 1), but more
212 importantly indicates that citrullination is a dynamic post-translational
213 modification of HP1γ with a potential role in regulating stem cell plasticity.
214
215 ***Mutations of HP1γ R38 and R39 do not affect soluble diffusion rate***
216 The positive charges of HP1γ R38 and R39 are important for binding to
217 H3K9me3 peptides *in vitro* (Fig 2). We then assessed whether citrullination of
218 R38 and R39 affects association of HP1γ to chromatin in live mESCs upon
219 LIF withdrawal. To analyze HP1γ dynamics *in vivo*, we used single-particle
220 tracking of HP1γ in mESCs cultured in presence and absence of LIF.
221 However, although HP1 dynamics have been well characterized using
222 numerous techniques over many years (26-29), the technique described here
223 has not previously been used to monitor the diffusion and binding kinetics of
224 HP1 molecules in live cells. Therefore, as a proof of principle, we tested this
225 technique by comparing wildtype HP1γ (HP1γWT) to the well-characterised
226 chromoshadow domain (CSD) mutant HP1γI165K, which prevents
227 dimerization of HP1γ (30). We generated mESC lines stably expressing HP1
228 N-terminally tagged with the photo-activatable fluorophore mEos3.2 (31)
229 fused to a HaloTag (32) (Fig 5A). Expression of fusion proteins was confirmed
230 by immunoblot analysis (Sup Fig 5A).
231
232 Tagged HP1γ molecules were labeled using low concentrations of HaloTag-
233 JF_{549} ligand (33) and dynamics were measured in mESCs at 13.5 ms time

234 resolution. Jump-distance analysis as illustrated in Fig 5A and B (34), showed
235 that both WT and CSD mutant molecules exhibit two major diffusion
236 coefficients (bound and diffusing) (Sup Fig 5B and C). This corresponds to
237 published results using fluorescence correlation spectroscopy (FCS) of GFP-
238 tagged HP1 proteins (28, 29). While diffusion coefficients of bound molecules
239 remained unchanged for HP1γI165K mutant proteins, diffusing mutant
240 molecules moved significantly more quickly than wildtype molecules (Sup Fig
241 5D to F, Table 2). Overall, these results confirm previously published
242 experiments employing fluorescence recovery after photobleaching (FRAP) of
243 HP1 CSD mutants in both heterochromatic as well as euchromatic regions *in*
244 *vivo* (26) and validate SPT as a suitable technique to detect differences in
245 HP1 mobility.
246
247 Given the success of the above proof of principle experiments, we next
248 compared mESCs (+/- LIF) expressing HP1γWT protein with cells expressing
249 HP1γR38/9A, mimicking citrullinated HP1γ. Importantly, exogenous
250 expression of HP1γ proteins had no discernible effect on mESC differentiation
251 as (i) ground state mRNA levels of the pluripotency markers (Sup Fig 4B); (ii)
252 down-regulation of mRNA levels of the pluripotency markers after LIF
253 withdrawal (Sup Fig 4C) and (iii) morphological changes after LIF withdrawal
254 (Sup Fig 4D) in mESCs stably expressing either HP1γWT or HP1γR38/9A
255 mutant proteins did not differ from those of parental mESCs.
256
257 We observed increased HP1γ foci formation in differentiating cells by
258 fluorescence imaging of mEos3.2 (Fig 5C), confirming a previous study using

259 the same differentiation protocol (35). However, no apparent difference was
260 detected between HP1γWT or HP1γR38/9A expressing cells. Similarly, SPT
261 analyses of either HP1γWT or HP1γR38/9A mutant proteins showed that LIF
262 withdrawal had no significant effect on their diffusion rate in mESCs (Fig 5D to
263 F, Table 2). These results indicate that the diffusion of soluble HP1γ
264 molecules is not affected by LIF withdrawal and it does not depend upon R38
265 and R39.
266
267 ***HP1γ R38 and R39 determine chromatin residence time in differentiating***
268 ***mESCs***
269 Although HP1 is a multifunctional protein, its best-characterized function is its
270 ability to specifically bind to H3 tails harboring H3K9me3. This underpins the
271 establishment of localized, as well as higher-order, chromatin domains.
272 Indeed, binding of structural chromatin proteins, such as HP1, is crucial in
273 establishing heterochromatin during stem cell differentiation (2). We therefore
274 decided to focus on the chromatin bound fraction of HP1γ. We used a concept
275 called motion blurring in which long exposures are used to blur molecules that
276 are diffusing so they are not detected. Therefore, only molecules bound
277 throughout the long exposure are imaged (32, 36, 37). We performed SPT at
278 500 ms time resolution of mESCs expressing either HP1γWT or HP1γR38/9A
279 mutant proteins (-/+ LIF). Movies of representative cells are shown in Movie 1
280 to 4. Motion blurring analysis revealed that HP1 molecules bound to
281 chromatin possess two main residence times which we will refer to as specific
282 and unspecific residence times (Fig 6A, Sup Fig 6, Table 2).
283

284 While LIF withdrawal had no effect on the unspecific residence time of either
285 HP1γWT or HP1γR38/9A molecules, the specific residence time of HP1γWT
286 molecules was significantly increased (20 sec longer upon differentiation, Fig
287 6B and D). In stark contrast, the specific residence time of R38/9A mutant
288 HP1γ molecules was considerably shorter (Fig 6B and D). Consequently, the
289 average time that HP1γR38/9A molecules remain stably bound to chromatin
290 in differentiating mESCs is significantly lower than for HP1γWT molecules
291 (29.5 +/- 4.1 vs. 49.2 +/- 12.3 s (Fig 6B and D)).
292
293 On the basis of these results we conclude that HP1γ residues R38 and R39
294 are not critical for HP1 recruitment to chromatin during stem cell
295 differentiation, because diffusion of soluble HP1γ molecules remained
296 unchanged upon LIF withdrawal. However, the two residues influence the
297 overall stability of HP1γ molecules bound to chromatin in differentiating
298 mESCs.
299

300 Discussion

301 Our findings are consistent with a model in which HP1γ in pluripotent mESCs
302 is citrullinated by PADI4 to reduce its affinity to chromatin (Fig 7). This may
303 explain, at least in part, how a relatively open chromatin conformation is
304 maintained in pluripotent mESCs. Upon differentiation, PADI4 expression
305 decreases (22) together with the levels of HP1γ citrullination (Fig 4D)
306 promoting its interaction with chromatin (increased specific residence time of
307 HP1γ - (Fig 6B and D)). This could help to establish heterochromatin domains

308 and/or regulate specific gene expression programs during stem cell
309 differentiation. Indeed, a similar non-mutually exclusive mechanism was
310 recently reported for H1, which is also citrullinated by PADI4 (22).

311 It will be difficult to determine whether HP1γ citrullination affects chromatin
312 domains in a long-range manner or whether it acts more locally, perhaps at
313 specific genes. However, our finding that PADI4 mediated citrullination of
314 HP1γ is significantly increased when HP1γ is bound to H3K9me3 peptides
315 supports the notion that HP1γ is targeted by the deiminase when bound to
316 chromatin. Thus, we hypothesize that HP1γ citrullination may represent a
317 relatively rare modification occurring at specific genomic loci to which PADI4
318 is recruited. Thus, HP1γ's residence time would be affected by citrullination at
319 specific genomic loci. In fact, our MS analysis assessed the stoichiometry of
320 HP1γ citrullination in mESCs to be in the very low percentage range, which
321 was supported by our immunoblotting experiments which detected low levels
322 of HP1γ citrullination in mESCs (Fig 4D). Given this, we believe that the
323 citrullination of HP1γ acts to regulate its chromatin binding at specific genomic
324 sites, possibly at genes controlling cellular plasticity.

325 Citrullination of histone H3R8 by PADI4 at gene promoters reduces the
326 binding affinity of HP1 to adjacent methylated H3K9 which results in gene
327 activation (38). It is possible that PADI4 targets both H3R8 and HP1γ bound
328 to the same H3 N-terminal tail. The *Nanog* gene may represent an important
329 example of such a locus, since chromatin immunoprecipitation experiments
330 have shown that both HP1γ and PADI4 bind to its promoter and regulate gene
331 expression in stem cells (16, 22).

332 Additional support of our model stems from a proteomics study demonstrating
333 HP1γ is predominantly nucleoplasmic in mESCs, with only a small fraction
334 stably bound to chromatin (39). In contrast, in cells with less pluripotent
335 potential, HP1γ is more chromatin bound and predominantly interacts with
336 H1(39), which itself is more chromatin bound (22) (Fig 7).

337 HP1 proteins possess domains that allow interaction with chromatin in a
338 multivalent fashion (reviewed in (40)). Here, we have shown that single
339 particle tracking can be used to reliably measure HP1 dynamics in live cells.
340 Given the significant increase in diffusion of fast moving HP1 molecules after
341 mutating the CSD, it is highly likely that HP1 molecules move and associate
342 with chromatin as dimers and/or as part of larger protein complexes. The
343 recently discovered ChAHP complex, comprised of transcription factor ADNP,
344 chromatin remodeler CHD4 and HP1, plays a crucial role in transcriptionally
345 regulating cell fate decisions (41). Hence, it will be interesting to investigate
346 how this protein complex affects HP1 dynamics in stem cells.
347
348 Finally, it is currently unclear whether citrullination of HP1γ is involved in the
349 reprogramming of cells to a more plastic state. However, this seems plausible
350 since loss of HP1γ increases the reprogramming efficiency of mouse
351 embryonic fibroblasts [16].
352

353 ## Conclusion

354 Our work identifies citrullination of HP1γ within its chromodomain as a novel
355 post-translational modification in mESCs. The modification affects the

356 protein's ability to bind H3K9me3 *in vitro* and chromatin *in vivo*. Importantly, it
357 is dynamically regulated during mESC differentiation. The arginines that are
358 citrullinated within the chromodomain directly influence the overall stability of
359 HP1γ molecules bound to chromatin in differentiating mESCs. Overall, our
360 data highlight citrullination of HP1γ as a mechanism facilitating mESC
361 differentiation.

362

363 ## Materials and Methods

364 **Mass spectrometry and identification of citrullinated peptides**

365 Previously published tandem mass spectrometry data of mESCs (22) was re-
366 analyzed using an improved search algorithm. Mass spectrometry data
367 analysis was performed with the MaxQuant software suite (version 1.2.6.20)
368 as described (43) supported by Andromeda (www.maxquant.org) as the
369 database search engine for peptide identifications (44). We followed the step-
370 by-step protocol of the MaxQuant software suite (45) to generate MS/MS
371 peak lists that were filtered to contain at most six peaks per 100 Da interval
372 and searched by Andromeda against a concatenated target/decoy (46)
373 (forward and reversed) version of the Uniprot human database version
374 (70.101 forward protein entries). Protein sequences of common contaminants
375 such as human keratins and proteases used were added to the database. The
376 initial mass tolerance in MS mode was set to 7 ppm and MS/MS mass
377 tolerance was set to 20 ppm. Cysteine carbamidomethylation was searched
378 as a fixed modification, whereas protein N-acetylation, oxidized methionine,
379 deamidation of asparagine and glutamine, and citrullination of arginines were

380 searched as variable modifications. A maximum of two miscleavages was
381 allowed while we required strict LysC specificity. Peptide assignments were
382 statistically evaluated in a Bayesian model on the basis of sequence length
383 and Andromeda score. We only accepted peptides and proteins with a false
384 discovery rate of less than 1%, estimated on the basis of the number of
385 accepted reverse hits.

386 Modification sites within peptide sequences were assigned by calculating the
387 localization post-translational modification (PTM) score, which is a probability-
388 based scoring system implemented in MaxQuant software suite and the
389 Andromeda search engine, described previously. The score is based on the
390 so-called MS3 scoring algorithm initially developed for the assignment of
391 phosphorylation sites (47). Briefly, the algorithm makes use of the 10 most
392 intense fragment ions per 100 amu in an acquired tandem mass MS/MS
393 spectrum. It then calculates the putative fragment ions (b- and y-ions for HCD
394 fragmentation) in the observed mass range for all possible combinations of
395 modification sites in a peptide sequence and determines the number of
396 matches, k. The localization PTM probability score is then derived based
397 upon $-10 \times \log_{10}(p)$, where the probability p is calculated as
398

$$p = \left(\frac{k!}{(n!\,(n-k)!}\right) \times pk \times (1-p)(n-k) = \left(\frac{k!}{(n!\,(n-k)!}\right) \times 0.04k$$

399 **Mammalian and bacterial expression constructs**

400 The vector pSB7 was generated from the pEF/*myc*/ER backbone (Invitrogen)
401 by replacing *myc*/ER regulatory elements with the sequence encoding

402 mEos3.2-HaloTag. Mouse HP1γ cDNA was cloned into Xho1/Xba1 restriction
403 sites of the mammalian expression vector pSB7 and into BamH1/EcoR1
404 restriction sites of the bacterial expression vector pGEX-2T. Point mutants
405 were generated using Quick change II site-directed mutagenesis kit
406 (Stratagene). Bacterial expression vector pGEX6p-GST-hPADI4 was
407 described previously (22).
408
409 **Immunoblotting and antibodies**
410 For immunoblotting, cells were lysed in 2x Laemmli buffer and sonicated in a
411 water-bath (Fisherbrand) for 3 min to shear genomic DNA, spun down at full
412 speed in a microfuge for 15 min and incubated for 5 min at 95 °C. Proteins
413 were resolved by SDS-PAGE, transferred to nitrocellulose membrane
414 (Millipore) using wet transfer (transfer buffer: 192 mM glycine, 25 mM Tris.HCl
415 pH8.8) and incubated in blocking solution (5% BSA in TBS containing 0.5%
416 Tween-20 for citrulline sensitive antibodies and 5% non-fat milk powder in
417 TBS containing 0.1% Tween-20 for all other antibodies) for 1 h at room
418 temperature (RT). Membranes were incubated with primary antibody at 4 °C
419 o/n and appropriate HRP-conjugated secondary antibody for 1 h at RT.
420 Membranes were then incubated for enhanced chemiluminescence (ECL,
421 Promega) and proteins were detected by exposure to X-ray film or using the
422 ChemiDoc™ MP imaging system (Bio-Rad). Images were quantified using
423 ImageJ analysis software. Primary antibodies, diluted in blocking solution
424 were used to detect citrullinated histone H3R2 (H3R2-Cit, Abcam ab176843
425 at 1:1000 dilution), HP1γ (Millipore 05-690 MAB clone 42s2 (16) at 1:1000
426 dilution), β-Tubulin (Abcam ab6046 at 1:1000 dilution) and peptidyl-citrulline

427 (Millipore MABN328, clone F95 (48) at 1:1000 dilution). HRP-conjugated
428 secondary antibodies diluted in blocking solution were used against mouse
429 IgG (Dako, P0447 at 1:5000 dilution) and rabbit IgG (Abcam, ab6721 at
430 1:20000 dilution).
431
432 **Immunoprecipitation**

433 mESCs were either cultured under Serum/LIF conditions or without LIF for 72
434 h. 2 X 10^7 cells were harvested, washed twice in ice cold 1xPBS and lysed in
435 1 ml of nuclear lysis buffer (NLB: 10 mM Hepes-KOH pH 7.9, 1.5 mM $MgCl_2$,
436 10 mM KCL, 0.5 mM DTT, 0.1% NP-40 Supplementaled with cOmplete^{TM}
437 proteinase inhibitor cocktail (Roche)). Lysate was incubated for 10 min on ice
438 and nuclei were pelleted at 2000 rpm for 10 min. Nuclear pellet was washed
439 in NLB and lysed in 0.5 ml 1x RIPA buffer (10mM Tris (pH 8.0), 1mM EDTA,
440 1% Triton X-100, 0.1% sodium deoxycholate, 0.1% SDS, 140mM NaCl)
441 Supplementaled with cOmplete^{TM} proteinase inhibitor cocktail (Roche)). The
442 lysate was incubated on ice for 20 min with vortexing every 5 min and
443 centrifuged at full speed for 15 min to remove cellular debris. 2 µg of HP1γ
444 antibody (Millipore 05-690 MAB clone 42s2) or an isotype control (Abcam,
445 HA.C5, ab18181) were added and incubated at 4 °C overnight on a rotating
446 wheel. 30 µl of Protein G Dynabeads® (Thermo Fisher Scientific) were added
447 and incubated for 2 h at 4 °C on a rotating wheel. Beads were washed 3x in
448 ice cold 1x RIPA, lysed in 2x Laemmli buffer, resolved by SDS-PAGE and
449 subjected to immunoblotting.

450

451 **Purification of recombinant GST-hPADI4 and *in vitro* deimination assay**

452 Recombinant human GST-PADI4 was expressed from pGEX6p constructs
453 (22) in LB_{Amp} media, induced with 0.1 mM IPTG at 30 °C for 4 h, purified using
454 glutathione-sepharose resin, eluted using a 25 mM glutathione solution and
455 stored in 20% glycerol at -20 °C. *In vitro* deimination of GST-HP1 variants was
456 carried out as described previously (22). *In vitro* deimination assays were
457 performed in the presence and absence of 100 ng H3(1-16) or H3K9me3
458 peptides as appropriate. Samples were resuspended in 1x Laemmli buffer for
459 immunoblot analysis.

460

461 **Bio-layer interferometry (BLI)**

462 Recombinant mouse full length HP1 wildtype and mutant proteins were
463 expressed in (as GST fusion proteins), and purified from, *Escherichia coli* as
464 described (4). Proteins were concentrated using Amicon Ultra centrifugation
465 filters with a 30 kDa cutoff (Milipore), washed into binding buffer (20 mM
466 Hepes-KOH pH 7.2, 70 mM KCl, 1 mM DTT, 0.1% Tween, 5% glycerol).
467 Protein concentrations were determined by Bradford protein assay against a
468 BSA standard and purity was verified by SDS-PAGE followed by Coomassie-
469 blue staining. Real-time binding assays of GST-HP1γ were performed using
470 the BLItz® system (ForteBio) in binding buffer (+0.1% BSA). Biotinylated
471 H3(1-16) peptides (NH_2-ARTKQTARK(me3)STGGKAP-Biotin) were
472 immobilized to Dip and Read High Precision Streptavidin (SAX) Biosensors
473 (ForteBio) and kinetics for a range of protein concentrations were measured
474 under advanced kinetics settings (1. initial baseline measuring buffer only: 30
475 s, 2. loading of peptides onto sensors: 120 s, 3. effective baseline

476 measurement: 30 s, 4. association of GST-HP1γ proteins: 120 s, 5.
477 dissociation of GST-HP1γ proteins: 120 s). The data were normalized to the
478 effective baseline signal by subtracting the average baseline value (150-180
479 s) from each data point (150 – 420s). Values of 1. and 2. measurements were
480 not included in analysis and are not displayed in figures. Raw data is
481 summarised in Table 1.
482
483 **Peptide pulldown assay**
484 H3K9me3 or unmethylated H3(1-16) peptides, linked to Dynabeads MyOne
485 streptavidin T1 (Thermo Fisher Scientific), were used in pulldown assays with
486 eluted GST-HP1 in HBS-EP (300 mM NaCl, 50 mM Tris-HCl pH 8.0, 5 mM
487 EDTA and 0.2% NP-40). Pull-down assays were performed in 300 mM NaCl
488 HBS-EP as previously described (4). Samples were resuspended in 2x
489 Laemmli buffer and resolved by SDS-PAGE followed by Coomassie-blue
490 staining. Images were quantified using ImageJ software.
491
492 **Cell culture**
493 Parental E14 mouse embryonic stem cell (mESC) line were profiled by
494 transcriptome analysis, qPCR and potency assays (22) and were routinely
495 tested for mycoplasma contamination and tested negative. Cells were
496 cultured in DMEM (Gibco) supplemented with 15% standard FCS (Gibco), 0.1
497 mM non-essential amino acids (Gibco), 1% penicillin/streptomycin, 2 mM L-
498 glutamine (Gibco), 1 mM sodium pyruvate (Gibco), 0.1 mM β-
499 mercaptoethanol (Life tech) and 10^6 units/L mLIF (ESGRO, Millipore). E14
500 cells were stored in incubators at 37 ^{o}C in 7.5% CO_2 (100% humidity) and

501 maintained in 0.1% gelatin coated 10 cm culture dishes with 1:6 passaging
502 every 2 days. Media was changed on a daily basis. E14 ESCs expressing
503 mouse mEos3.2-HaloTag-HP1 fusion proteins were generated by transfecting
504 appropriate pSB7 plasmids into E14 cells using Lipofectamine 2000
505 transfection reagent (Invitrogen), followed by selection in 600 µg/ml geneticin
506 (Life Technologies). After 2 weeks of geneticin selection, cells were sorted
507 using a Sony SH800S cell sorter for the expression of mEos3.2.
508 Differentiation of ESCs was induced by LIF withdrawal. ESCs cultured in
509 complete ES cell media (+ LIF) were trypsinised and washed twice in 1x PBS
510 to remove residual LIF, seeded into ES cell media without LIF and incubated
511 for 24, 48 or 72 h.
512
513 **cDNA synthesis and RT-PCR**
514 Cells were lysed using QIAzol® lysis reagent (Qiagen) and total RNA was
515 isolated using RNeasy® Mini Kit with in column DNase treatment (Qiagen).
516 1µg of total RNA was reverse transcribed using Superscript III Reverse
517 Transcriptase kit (Invitrogen). Samples were diluted 1:10 in nuclease-free
518 water prior to RT-PCR analysis. RT-PCR reactions were performed in
519 duplicates for each sample. Each RT-PCR reaction was performed in a final
520 volume of 10 µl. Fast SYBR Green Master Mix (Applied Biosystems) was
521 used, according to the manufacturer's instructions. A melting curve was
522 obtained for each PCR product after each run, in order to confirm that the
523 SYBR Green signal corresponded to a unique and specific amplicon. Relative
524 expression was calculated with the $2^{-\Delta\Delta Ct}$ method, normalizing to the

525 housekeeping gene β-actin. Data were analyzed using GraphPad Prism 7
526 software. Primers used in this study are summarized in Table 3.
527
528 **Microscope setup**
529 An IX73 Olympus inverted microscope was used with circularly polarized laser
530 beams aligned and focused at the back aperture of an Olympus 1.40 NA 100×
531 oil objective (Universal Plan Super Apochromat, 100x, NA 1.40,
532 UPLSAPO100XO/1.4). Continuous wavelength diode laser light sources used
533 include a 561 nm (Cobolt, Jive 200, 200 mW) and a 405 nm laser (Stradus,
534 Toptica, 405-100, 100 mW). Oblique angle illumination was achieved by
535 aligning the laser off axis such that the emergent beam at the sample
536 interface was near-collimated and incident at an angle slightly less than the
537 critical angle θ_c ~ 67° for a glass/water interface. This generated a ~50 μm
538 diameter excitation footprint. The power of the collimated beams at the back
539 aperture of the microscope was 10 kW/cm^2 and 10-100 W/cm^2 for the 561 nm
540 and 405 nm laser beams respectively. The lasers were reflected by dichroic
541 mirrors (Semrock, Di01- R405/488/561/635). The fluorescence emission was
542 collected through the same objective and then further filtered using a
543 combination of long-pass and band-pass filters (BLP01-561R and FF01-
544 587/35 for 561 nm excitation). The emission signal was projected onto an
545 EMCCD (Photometrics, Evolve 512 Delta) with an electron multiplication gain
546 of 250 ADU/photon operating in a frame transfer mode. The instrument was
547 automated using the open-source software micro-manager (49) and the data
548 displayed using the ImageJ software.
549

550 **Mammalian live-cell single-molecule imaging and analysis**

551 mESCs expressing mEos3.2-HaloTag-tagged HP1γ were passaged two days
552 before imaging onto 35 mm glass bottom dishes No 1.0 (MatTek Corporation
553 P35G-1.0-14-C Case) in phenol red-free serum and LIF conditions, if not
554 stated otherwise. Just before single-particle tracking (SPT) imaging
555 experiments, cells were labeled with 0.5 nM HaloTag-JF_{549} ligand for at least
556 15 minutes, followed by two washes in PBS and a 30-minute incubation at 37
557 °C in media, before imaging the cells in fresh phenol red-free serum and LIF
558 conditions. Cells were under-labeled to prevent overlap of fluorophores during
559 SPT. Using 561 nm excitation, fluorescence images were collected as movies
560 of 10,000 frames at 13.5 ms or 1,000 to 5,000 frames at 500 ms exposure.
561 For live-cell tracking, data was collected for three biological replicates on
562 separate dishes and the average values compared. Experiments carried out
563 on two separate days showed similar trends.

564

565 Live-cell 13.5 ms single-molecule traces were analyzed using software that
566 detects single-molecule trajectories from SPT movies (34). Briefly, the code
567 detected puncta positions in each image frame using a brightness-weighted
568 centroid after applying a band-pass filter to remove low-frequency background
569 and high-frequency noise from the image data. To track the HP1 single-
570 molecules, only fluorescent puncta smaller than 3 pixels and with a signal-to-
571 noise greater than 8 were analyzed. Fluorescent puncta were considered to
572 be the same molecule if they were within 6 pixels (936 nm) between frames.
573 We collected more than 5,000 single-molecule trajectories from single-
574 molecule movies of HP1γWT, HP1γI165K and HP1γR38/9A molecules

575 detected within an ROI of an average of 3-4 cells. Given we observed an
576 increase in diffusion coefficient of the fast sub-population of HP1WT
577 molecules compared to the CSD mutants (63% of molecules for HP1γWT),
578 this is an appropriate sample size to demonstrate the change we observe.
579 13.5 ms SPT experiment (i) was recorded in one day and repeat experiments
580 (n=2-9, number of replicates varies between cell lines) were recorded on a
581 different day over the course of 5 days. 500 ms data repeat experiments (n=3)
582 were recorded on three different days. Independent replicates were compared
583 using two-way ANOVA multiple corrections with Sidak *post hoc* test. This is
584 justified because the variances calculated were similar between samples.
585
586 Live cell 500 ms single molecule traces were analyzed using Rapidstorm
587 software that determines single-molecule localizations from PALM movies
588 (50), after using ImageJ's rolling back background correction with a radius of
589 5 pixels. Only fluorescent puncta less than 3 pixels wide with a fixed global
590 threshold above 25000 were analyzed. We collected more than 1,000 single-
591 molecule trajectories from single-molecule movies of HP1γWT and
592 HP1γR38/9A molecules before and after mESC differentiation. Given we
593 observed an increase in the residence time of the stable binding HP1γWT
594 molecules (10-13% of molecules), this is an appropriate sample size to
595 demonstrate the change we observe.
596
597 Data was fit 1000 times after which the mean of the parameters estimated
598 using the parametric bootstrap model:
599 $F(t) = \mathbf{\Sigma}\, f_i \exp(-t/\tau_i)$

600 , where f_i is the fraction of molecules with a residence time of τ_i. For example,
601 a two-component fit was fit to the equation:
602 $F(t) = f_1\exp(-t/\tau_1) + (1-f_1)\exp(-t/\tau_2)$
603 , where f_1 and $(1-f_1)$ are the percentage of molecules with residence times of
604 tau1 and tau2.
605
606 The code is provided on Github. We determined the relative likelihood for
607 each model for each data set by use of the Bayesian Information Criterion
608 (BIC) (51) as previously described for the case of comparing different diffusion
609 models for single particle tracking data (52). In short, using this approach we
610 calculated the BIC for each model from:

$$BIC = \ln\,[n](p+1) + n\left(\ln\left[\frac{2\,\pi\,RSS}{n}\right] + 1\right)$$

611 , where n is the number of data points, p is the number of free parameters for
612 the fit, and RSS is the residual sum of squares of the fit. The fit with the lowest
613 BIC was used (Sup Fig 6). The average values were then calculated from the
614 fits of three independent biological replicates and compared. A Z-test was
615 used to calculate the p-values because the means are normally distributed
616 and showed similar variance.
617

618 **Figure Legends**

619 **Figure 1:**

620 ***HP1γ chromodomain is citrullinated in vivo***

621 **A** The left panel is a schematic illustration of the functional domain structure
622 of mouse HP1γ. Chromodomain (CD, blue), hinge region (HR, orange),

623 chromoshadow domain (CSD, green) and N-terminal extension (grey) are
624 indicated. Above is a multiple sequence alignment of mouse HP1 paralogue
625 chromodomain amino acid (aa) sequences using Clustal Omega. CD
626 secondary structures are indicated above the sequences and residues
627 forming the hydrophobic H3K9me3 binding pocket (5) are highlighted in
628 turquois. Citrullinated residues are highlighted in pink. The right panel shows
629 an X-ray crystal structure of the HP1γ CD in complex with H3K9me3. PDB file
630 '5tli' was adapted using Pymole. Residues forming the hydrophobic pocket
631 are highlighted in turquois and citrullinated residues in pink.
632 **B/C** MS/MS analysis identifies citrullination of HP1γ at residues R38 and/or
633 R39 in a chromatin fraction of mESCs. Plots show the fragmentation spectra
634 of the LysC peptides VLDRRVVNGKVEYELK (**B**) and VLDRRVVNGK (**C**)
635 surrounding arginine (R) 38 and R39 of HP1γ. The y (red) and b (blue) series
636 indicate fragments at amide bonds of the peptide. Immonium ions unique for
637 citrulline (Im/(Cit) at m/z 130) and arginine (Im/(Arg) at m/z 129) were
638 detected in both peptides.
639

640 **Figure 2:**

641 ***Loss of charge at residues R38 and R39 impairs HP1γ binding to***
642 ***H3K9me3 in vitro***

643 **A** Coomassie-blue stained gel showing the results from a pulldown assay
644 analysing binding of recombinant GST-HP1γWT and GST-HP1γR38/9A
645 proteins to H3(1-16) peptides or H3K9me3(1-16) peptides, as indicated. 25%
646 of input amounts are shown. Binding intensities of gel bands from multiple
647 experiments (Sup Fig 2A) were quantified using ImageJ and were normalized

648 to total inputs (right hand graph). Statistical analysis was performed using
649 unpaired, 2 tailed Student's t-test. Bars represent ± SD, n=3 (*p-value: 0.021,
650 **p-value: 0.008, ns.: not significant, p-value: 0.181). The sequences of the
651 peptides used are indicated at the top.
652 **B** Real-time binding kinetics of GST-HP1γ proteins using bio-layer
653 interferometry (BLI). BLI sensorgrams are shown profiling the normalized
654 binding of recombinant GST-HP1γWT and GST-HP1γR38/9A to H3(1-16)
655 peptides (H3: right panel) and H3K9me3(1-16) peptides (H3K9me3: left
656 panel), as indicated. Association (30-150 s) and dissociation (150-270 s) were
657 each measured over the course of 120 s. The protein concentrations used
658 were WT: 28.0 μM; R38/9A: 28.3 μM. Results of one experiment repeated at
659 a range of different protein concentrations are shown (Sup Fig 2C.
660

661 **Figure 3:**

662 ***PADI4 citrullinates HP1γ in vitro***

663 **A** Recombinant GST-HP1γWT, R38K, R39K or R38/9K mutant proteins were
664 incubated with recombinant GST-PADI4 in the presence or absence of
665 activating calcium as indicated. Reactions were resolved by SDS-PAGE and
666 analyzed by immunoblot analysis using an anti-peptidyl-citrulline antibody.
667 Ponceau S staining of the transferred proteins serves as a loading control
668 (lower panel). Bands highlighted by the red boxes were quantified using
669 ImageJ. Total intensities after background correction are indicated (right
670 panel). Statistical analysis was performed using two-way ANOVA multiple
671 corrections with Sidak *post hoc* test. Bars represent ± SD, n=3 (**p-values
672 from left to right: 0.002, 0.003, 0.008) (Sup Fig 3A).

673 **B** GST-HP1γWT or R38/9K mutant proteins were incubated with GST-PADI4,
674 with or without calcium, in the presence or absence (w/o) of unmethylated H3
675 (1-16) peptides or H3K9me3(1-16) peptides, as indicated. Ponceau S staining
676 of the transferred proteins serves as a loading control (lower panel). Bands
677 highlighted by the red boxes were quantified using ImageJ and background
678 corrected. Increased citrullination of HP1γWT in the presence of H3K9me3
679 peptides compared to unmethylated H3 peptide is displayed as fold change
680 intensity (right panel). Statistical analysis was performed using unpaired
681 Student's t test. Bars represent ± SD, n=3 (**p-value: 0.004) (Sup Fig 3B).

682 **Figure 4:**

683 ***HP1γ citrullination is reduced in differentiating mESCs***

684 **A** Schematic illustration of differentiation experiments. mESCs were cultured
685 in the presence (+LIF) or absence of LIF (-LIF) for 24, 48 and 72 hours.
686 Experiments were performed at 72h.

687 **B** mRNA levels of pluripotency markers in mESCs decrease after withdrawal
688 of LIF. The mRNA levels of the indicated genes were measured by RT-PCR
689 over a course of 3 days after withdrawal of LIF. RT-PCR data were
690 normalized to *β-actin* mRNA expression and expression fold-change was
691 determined relative to d_0 time point using the ddCT method. Bars represent ±
692 SEM, n=2.

693 **C** Representative lightfield microscope images of mESCs before and after 72
694 h LIF withdrawal, captured with a Leica EC3 camera at 20x magnification.
695 Scale bars: 100 μm.

696 **D** Immunoprecipitation (IP) of endogenous HP1γ from nuclear lysates of
697 mESCs cultured +/- LIF for 72h. IPs were performed with anti-HP1γ
698 antibodies (α-HP1γ) and anti-HA control antibodies and analyzed by
699 immunoblotting using an anti-peptidyl-citrulline antibody (α-Citrulline). The
700 same immunoblot was re-probed with an α-HP1γ antibody. 4% input of each
701 IP is indicated. An uncropped image together with two more replicates is
702 shown in Sup Fig 4A.

703 **Figure 5:**

704 ***Mutation of HP1γ R38 and R39 does not affect diffusion rate of diffusing***
705 ***molecules***

706 Statistical analyses were performed using two-way ANOVA multiple
707 corrections with Sidak *post hoc* test. mESCs were cultured +/- LIF for 72h.

708 **A** Schematic illustration of mEos3.2-HaloTag-HP1 fusion proteins used for
709 single-particle tracking (left panel). X-ray crystal structures of green EosFP
710 (PDB_1ZUX) and HaloTag (PDB_5UXZ) are shown together with the
711 chemical structure of JF_{549} dye coupled to the HaloTag-chloroalkane linker.
712 Right panel shows schematic illustration of jump distance (JD) analysis of
713 single particle tracking (SPT) data to determine diffusion coefficients (D). JD
714 analysis plots a histogram of all particle displacements within a fixed time
715 interval Δt for all trajectories. Fitting the distribution of displacements yields
716 the minimum number of diffusion coefficients needed to describe the motion
717 of the particles.

718 **B** Representative mEos3.2 fluorescent images at 488 nm excitation of
719 mESCs expressing mEos3.2-HaloTag-HP1WT and single molecule tracks of

720 HaloTag-JF_{549}-tagged molecules are shown. Scale bar: 2 µm. Bound and
721 diffusing molecules are highlighted.
722 **C** Representative mEos3.2 fluorescent images of mESCs expressing
723 mEos3.2-HaloTag- HP1γWT and HP1γR38/9A. Scale bar: 2 µm.
724 **D/E** SPT of mEos3.2-HaloTag- HP1γWT and HP1γR38/9A in mESCs. **D** Cells
725 were labeled with HaloTag-JF_{549} ligand and subjected to 2D SPT. At 561 nm
726 fluorescent images were collected as movies of 10000 frames at 13.5 ms time
727 resolution. Plot depicts diffusion coefficients (D) [$\mu m^2 s^{-1}$] of the indicated HP1
728 molecules. Bars represent ± SD (n=5-9). Multiple comparisons resulted in no
729 significant differences across conditions (ns. p-values > 0.999). **E**
730 Percentages of molecules within diffusing and bound fractions (ns. p-values >
731 0.967).
732 **F** Tabulated summary of results shown in **D** and **E.**
733

734 **Figure 6:**

735 ***HP1γ R38 and R39 influence chromatin residence time in differentiating***
736 ***mESCs***

737 Statistical analyses were performed using two-way ANOVA multiple
738 corrections with Sidak *post hoc* test. mESCs were cultured +/- LIF for 72h.
739 **A** Schematic illustration of HP1γ dynamics in mESCs. SPT of mEos3.2-
740 HaloTag-HP1γ molecules at 13.5 ms time resolution determines two fractions
741 with individual diffusion coefficients: diffusing and bound. SPT at 500 ms time
742 resolution allows further detection of molecule dynamics within the bound
743 fraction (~37.4% of all detectable HP1γ molecules). Within the bound fraction,

744 two populations with individual residence times (t_{res}) [s] are detected:
745 unspecific (t_{res} = 2.4 s) and specific (t_{res} = 28.8 s).
746 **B/C** SPT of mEos3.2-HaloTag-HP1γWT and HP1γR38/9A in mESCs. **B** Cells
747 were labeled with HaloTag-JF_{549} ligand and subjected to SPT. At 561 nm
748 fluorescent images were collected as movies of 1000 frames at 500 ms time
749 resolution. Left panel depicts the t_{res} for specific and unspecific binding of the
750 indicated HP1 molecules. Bars represent ± SD (n=3) (*: p-value left to right =
751 0.027, 0.036; ns. p-value > 0.841). **C** Percentages of molecules with
752 unspecifc and specific t_{res}.
753 **D** Tabulated summary of results shown in **B** and **C.** Errors represent ± SD
754 (n=3).
755

756 **Figure 7:**

757 Working model depicting a role for HP1γ R38 and R39 during stem cell
758 differentiation. In pluripotent stem cells, HP1γ proteins bound to specific
759 genomic loci (e.g. *Nanog* promoter) are citrullinated (cit) by PADI4 to reduce
760 their affinity to chromatin, whilst the diffusion of soluble HP1γ molecules is not
761 affected. This may explain, at least in part, how a relatively open chromatin
762 conformation at specific gene loci and expression of pluripotency genes in
763 stem cells is maintained. A similar (non-mutually exclusive) mechanism was
764 identified for H1 (22), which interacts with HP1γ in stem cells with reduced
765 pluripotent potential (39). Upon differentiation, PADI4 expression decreases
766 and the subsequent reduction in HP1γ citrullination would promote its
767 interaction with chromatin (increased specific residence time), resulting in
768 chromatin compaction and/or changes in gene expression.

Declarations

Availability of data and material

The datasets generated and analyzed during the current study as well as materials are available from the authors on request. The software used for live-cell diffusion analysis and residence time analysis can be found at https://github.com/TheLaueLab/weimann-tracking and https://github.com/TheLaueLab/trajectory-analysis respectively. Other software used include the open-source software micro-manager (https://www.micro-manager.org), ImageJ (53, 54), Rapidstorm (50) and PeakFit (55).

Competing interests

T.K. is a co-founder of Abcam plc (Cambridge, UK).

Funding

The Kouzarides laboratory is supported by a grant from Cancer Research UK (grant reference RG17001) in addition to benefiting from core support from the Wellcome Trust (Core Grant reference WT203144) and Cancer Research UK (grant reference C6946/A24843). The Laue laboratory is supported by grants from the Wellcome Trust (206291/Z/17/Z) and the Medical Research Council (MR/P019471/1 and MR/M010082/1). M.L.N was partly supported by the Novo Nordisk Foundation Center for Protein Research, the Lundbeck Foundation, and by and the European Commission's 7th Framework Programme HEALTH-F7-2010-242129/SYBOSS. David Klenerman is

supported by a Royal Society Professorship (RP150066) and the microscope used for single particle tracking experiments was funded by the MRC (MR/K015850/1).

Author contributions

M.W. and A.J.B. designed experiments and interpreted results. M.W. carried out all *in vitro* experiments, generated cell lines and prepared samples for imaging analysis. S.B. performed SPT experiments and data analysis with help of W.B. and K.W. SPT experiments were carried out using instrumentations in D.K.'s laboratory. Mass spectrometry data was generated and analyzed by M.A.C. and M.L.N.. T.K., S.B. and E.D.L. supervised the project. M.W. and A.J.B. wrote the manuscript with contributions from all authors.

Acknowledgements

We thank Dr. Claudia Keller Valsecchi for help setting up the BLI experiments and Dr. Asifa Akhtar for providing access to equipment in her laboratory. We thank Dr. Valentina Migliori for proof reading the manuscript and helpful comments.

References

1. Meshorer E, Misteli T. Chromatin in pluripotent embryonic stem cells and differentiation. Nat Rev Mol Cell Biol. 2006;7(7):540-6.
2. Meshorer E, Yellajoshula D, George E, Scambler PJ, Brown DT, Misteli T. Hyperdynamic plasticity of chromatin proteins in pluripotent embryonic stem cells. Dev Cell. 2006;10(1):105-16.

819 3. Eissenberg JC, Morris GD, Reuter G, Hartnett T. The heterochromatin-
820 associated protein HP-1 is an essential protein in Drosophila with dosage-
821 dependent effects on position-effect variegation. Genetics. 1992;131(2):345-
822 52.
823 4. Bannister AJ, Zegerman P, Partridge JF, Miska EA, Thomas JO,
824 Allshire RC, et al. Selective recognition of methylated lysine 9 on histone H3
825 by the HP1 chromo domain. Nature. 2001;410(6824):120-4.
826 5. Nielsen PR, Nietlispach D, Mott HR, Callaghan J, Bannister A,
827 Kouzarides T, et al. Structure of the HP1 chromodomain bound to histone H3
828 methylated at lysine 9. Nature. 2002;416(6876):103-7.
829 6. Maison C, Almouzni G. HP1 and the dynamics of heterochromatin
830 maintenance. Nat Rev Mol Cell Biol. 2004;5(4):296-304.
831 7. Smallwood A, Hon GC, Jin F, Henry RE, Espinosa JM, Ren B. CBX3
832 regulates efficient RNA processing genome-wide. Genome Res.
833 2012;22(8):1426-36.
834 8. Vakoc CR, Mandat SA, Olenchock BA, Blobel GA. Histone H3 lysine 9
835 methylation and HP1gamma are associated with transcription elongation
836 through mammalian chromatin. Mol Cell. 2005;19(3):381-91.
837 9. Lomberk G, Bensi D, Fernandez-Zapico ME, Urrutia R. Evidence for
838 the existence of an HP1-mediated subcode within the histone code. Nat Cell
839 Biol. 2006;8(4):407-15.
840 10. Harouz H, Rachez C, Meijer BM, Marteyn B, Donnadieu F, Cammas F,
841 et al. Shigella flexneri targets the HP1gamma subcode through the
842 phosphothreonine lyase OspF. EMBO J. 2014;33(22):2606-22.
843 11. Thorne JL, Ouboussad L, Lefevre PF. Heterochromatin protein 1
844 gamma and IkappaB kinase alpha interdependence during tumour necrosis
845 factor gene transcription elongation in activated macrophages. Nucleic Acids
846 Res. 2012;40(16):7676-89.
847 12. Saint-Andre V, Batsche E, Rachez C, Muchardt C. Histone H3 lysine 9
848 trimethylation and HP1gamma favor inclusion of alternative exons. Nat Struct
849 Mol Biol. 2011;18(3):337-44.
850 13. Morikawa K, Ikeda N, Hisatome I, Shirayoshi Y. Heterochromatin
851 protein 1gamma overexpression in P19 embryonal carcinoma cells elicits
852 spontaneous differentiation into the three germ layers. Biochem Biophys Res
853 Commun. 2013;431(2):225-31.
854 14. Huang C, Su T, Xue Y, Cheng C, Lay FD, McKee RA, et al. Cbx3
855 maintains lineage specificity during neural differentiation. Genes Dev.
856 2017;31(3):241-6.
857 15. Caillier M, Thenot S, Tribollet V, Birot AM, Samarut J, Mey A. Role of
858 the epigenetic regulator HP1gamma in the control of embryonic stem cell
859 properties. PLoS One. 2010;5(11):e15507.
860 16. Sridharan R, Gonzales-Cope M, Chronis C, Bonora G, McKee R,
861 Huang C, et al. Proteomic and genomic approaches reveal critical functions of
862 H3K9 methylation and heterochromatin protein-1gamma in reprogramming to
863 pluripotency. Nat Cell Biol. 2013;15(7):872-82.
864 17. Wang S, Wang Y. Peptidylarginine deiminases in citrullination, gene
865 regulation, health and pathogenesis. Biochim Biophys Acta.
866 2013;1829(10):1126-35.

867 18. Wang Y, Wysocka J, Sayegh J, Lee YH, Perlin JR, Leonelli L, et al.
868 Human PAD4 regulates histone arginine methylation levels via
869 demethylimination. Science. 2004;306(5694):279-83.
870 19. Zhang X, Bolt M, Guertin MJ, Chen W, Zhang S, Cherrington BD, et al.
871 Peptidylarginine deiminase 2-catalyzed histone H3 arginine 26 citrullination
872 facilitates estrogen receptor alpha target gene activation. Proc Natl Acad Sci
873 U S A. 2012;109(33):13331-6.
874 20. Zhang X, Liu X, Zhang M, Li T, Muth A, Thompson PR, et al.
875 Peptidylarginine deiminase 1-catalyzed histone citrullination is essential for
876 early embryo development. Sci Rep. 2016;6:38727.
877 21. Cuthbert GL, Daujat S, Snowden AW, Erdjument-Bromage H,
878 Hagiwara T, Yamada M, et al. Histone deimination antagonizes arginine
879 methylation. Cell. 2004;118(5):545-53.
880 22. Christophorou MA, Castelo-Branco G, Halley-Stott RP, Oliveira CS,
881 Loos R, Radzisheuskaya A, et al. Citrullination regulates pluripotency and
882 histone H1 binding to chromatin. Nature. 2014;507(7490):104-8.
883 23. Bryan LC, Weilandt DR, Bachmann AL, Kilic S, Lechner CC, Odermatt
884 PD, et al. Single-molecule kinetic analysis of HP1-chromatin binding reveals a
885 dynamic network of histone modification and DNA interactions. Nucleic Acids
886 Res. 2017;45(18):10504-17.
887 24. Deplus R, Denis H, Putmans P, Calonne E, Fourrez M, Yamamoto K,
888 et al. Citrullination of DNMT3A by PADI4 regulates its stability and controls
889 DNA methylation. Nucleic Acids Res. 2014;42(13):8285-96.
890 25. Tanikawa C, Ueda K, Suzuki A, Iida A, Nakamura R, Atsuta N, et al.
891 Citrullination of RGG Motifs in FET Proteins by PAD4 Regulates Protein
892 Aggregation and ALS Susceptibility. Cell Rep. 2018;22(6):1473-83.
893 26. Cheutin T, McNairn AJ, Jenuwein T, Gilbert DM, Singh PB, Misteli T.
894 Maintenance of stable heterochromatin domains by dynamic HP1 binding.
895 Science. 2003;299(5607):721-5.
896 27. Festenstein R, Pagakis SN, Hiragami K, Lyon D, Verreault A, Sekkali
897 B, et al. Modulation of heterochromatin protein 1 dynamics in primary
898 Mammalian cells. Science. 2003;299(5607):719-21.
899 28. Schmiedeberg L, Weisshart K, Diekmann S, Meyer Zu Hoerste G,
900 Hemmerich P. High- and low-mobility populations of HP1 in heterochromatin
901 of mammalian cells. Mol Biol Cell. 2004;15(6):2819-33.
902 29. Muller KP, Erdel F, Caudron-Herger M, Marth C, Fodor BD, Richter M,
903 et al. Multiscale analysis of dynamics and interactions of heterochromatin
904 protein 1 by fluorescence fluctuation microscopy. Biophys J.
905 2009;97(11):2876-85.
906 30. Mishima Y, Jayasinghe CD, Lu K, Otani J, Shirakawa M, Kawakami T,
907 et al. Nucleosome compaction facilitates HP1gamma binding to methylated
908 H3K9. Nucleic Acids Res. 2015;43(21):10200-12.
909 31. Zhang M, Chang H, Zhang Y, Yu J, Wu L, Ji W, et al. Rational design
910 of true monomeric and bright photoactivatable fluorescent proteins. Nat
911 Methods. 2012;9(7):727-9.
912 32. Chen J, Zhang Z, Li L, Chen BC, Revyakin A, Hajj B, et al. Single-
913 molecule dynamics of enhanceosome assembly in embryonic stem cells. Cell.
914 2014;156(6):1274-85.

915 33. Grimm JB, English BP, Chen J, Slaughter JP, Zhang Z, Revyakin A, et
916 al. A general method to improve fluorophores for live-cell and single-molecule
917 microscopy. Nat Methods. 2015;12(3):244-50, 3 p following 50.
918 34. Weimann L, Ganzinger KA, McColl J, Irvine KL, Davis SJ, Gay NJ, et
919 al. A quantitative comparison of single-dye tracking analysis tools using Monte
920 Carlo simulations. PLoS One. 2013;8(5):e64287.
921 35. Dialynas GK, Terjung S, Brown JP, Aucott RL, Baron-Luhr B, Singh
922 PB, et al. Plasticity of HP1 proteins in mammalian cells. J Cell Sci.
923 2007;120(Pt 19):3415-24.
924 36. Etheridge TJ, Boulineau RL, Herbert A, Watson AT, Daigaku Y, Tucker
925 J, et al. Quantification of DNA-associated proteins inside eukaryotic cells
926 using single-molecule localization microscopy. Nucleic Acids Res.
927 2014;42(19):e146.
928 37. Gebhardt JC, Suter DM, Roy R, Zhao ZW, Chapman AR, Basu S, et al.
929 Single-molecule imaging of transcription factor binding to DNA in live
930 mammalian cells. Nat Methods. 2013;10(5):421-6.
931 38. Sharma P, Azebi S, England P, Christensen T, Moller-Larsen A,
932 Petersen T, et al. Citrullination of histone H3 interferes with HP1-mediated
933 transcriptional repression. PLoS Genet. 2012;8(9):e1002934.
934 39. Zaidan NZ, Walker KJ, Brown JE, Schaffer LV, Scalf M, Shortreed MR,
935 et al. Compartmentalization of HP1 Proteins in Pluripotency Acquisition and
936 Maintenance. Stem Cell Reports. 2018;10(2):627-41.
937 40. Canzio D, Larson A, Narlikar GJ. Mechanisms of functional promiscuity
938 by HP1 proteins. Trends Cell Biol. 2014;24(6):377-86.
939 41. Ostapcuk V, Mohn F, Carl SH, Basters A, Hess D, Iesmantavicius V, et
940 al. Activity-dependent neuroprotective protein recruits HP1 and CHD4 to
941 control lineage-specifying genes. Nature. 2018;557(7707):739-43.
942 42. Lee YH, Coonrod SA, Kraus WL, Jelinek MA, Stallcup MR. Regulation
943 of coactivator complex assembly and function by protein arginine methylation
944 and demethylimination. Proc Natl Acad Sci U S A. 2005;102(10):3611-6.
945 43. Cox J, Mann M. MaxQuant enables high peptide identification rates,
946 individualized p.p.b.-range mass accuracies and proteome-wide protein
947 quantification. Nat Biotechnol. 2008;26(12):1367-72.
948 44. Cox J, Neuhauser N, Michalski A, Scheltema RA, Olsen JV, Mann M.
949 Andromeda: a peptide search engine integrated into the MaxQuant
950 environment. J Proteome Res. 2011;10(4):1794-805.
951 45. Cox J, Matic I, Hilger M, Nagaraj N, Selbach M, Olsen JV, et al. A
952 practical guide to the MaxQuant computational platform for SILAC-based
953 quantitative proteomics. Nat Protoc. 2009;4(5):698-705.
954 46. Elias JE, Gygi SP. Target-decoy search strategy for increased
955 confidence in large-scale protein identifications by mass spectrometry. Nat
956 Methods. 2007;4(3):207-14.
957 47. Olsen JV, Mann M. Improved peptide identification in proteomics by
958 two consecutive stages of mass spectrometric fragmentation. Proceedings of
959 the National Academy of Sciences of the United States of America.
960 2004;101(37):13417-22.
961 48. Nicholas AP, Whitaker JN. Preparation of a monoclonal antibody to
962 citrullinated epitopes: its characterization and some applications to
963 immunohistochemistry in human brain. Glia. 2002;37(4):328-36.

964 49. Edelstein AD, Tsuchida MA, Amodaj N, Pinkard H, Vale RD, Stuurman
965 N. Advanced methods of microscope control using muManager software. J
966 Biol Methods. 2014;1(2).
967 50. Wolter S, Loschberger A, Holm T, Aufmkolk S, Dabauvalle MC, van de
968 Linde S, et al. rapidSTORM: accurate, fast open-source software for
969 localization microscopy. Nat Methods. 2012;9(11):1040-1.
970 51. Schwarz G. Estimating the Dimension of a Model. Ann Statist.
971 1978;6(2):461-4.
972 52. Lagerholm BC, Andrade DM, Clausen MP, Eggeling C. Convergence
973 of lateral dynamic measurements in the plasma membrane of live cells from
974 single particle tracking and STED-FCS. J Phys D Appl Phys.
975 2017;50(6):063001.
976 53. Schneider CA, Rasband WS, Eliceiri KW. NIH Image to ImageJ: 25
977 years of image analysis. Nature methods. 2012;9(7):671-5.
978 54. Edelstein A, Amodaj N, Hoover K, Vale R, Stuurman N. Computer
979 control of microscopes using microManager. Curr Protoc Mol Biol.
980 2010;Chapter 14:Unit14 20.
981 55. Herbert A. 2014:Peak Fit, a Single-molecule Plugins. Available at
982 http://www.sussex.ac.uk/gdsc/intranet/microscopy/imagej/smlm_plugins.
983

Figure 1

A

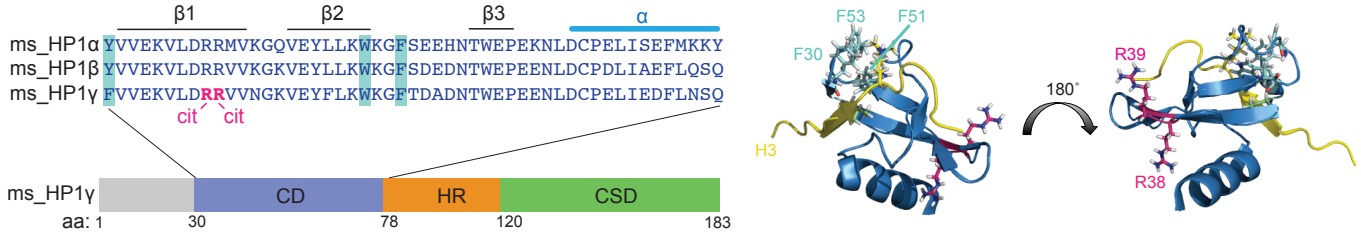
β1
β2
β3
α
ms_HP1α YVVEKVLDRRMVKGQVEYLLKWKGFSEEHNTWEPEKNLDCPELISEFMKKY
ms_HP1β YVVEKVLDRRVVKGKVEYLLKWKGFSDEDNTWEPEENLDCPDLIAEFLQSQ
ms_HP1γ FVVEKVLDRRVVNGKVEYFLKWKGFTDADNTWEPEENLDCPELIEDFLNSQ
cit
cit
ms_HP1γ
CD
HR
CSD
aa: 1
30
78
120
183
F53
F51
F30
H3
180˚
R39
R38

B

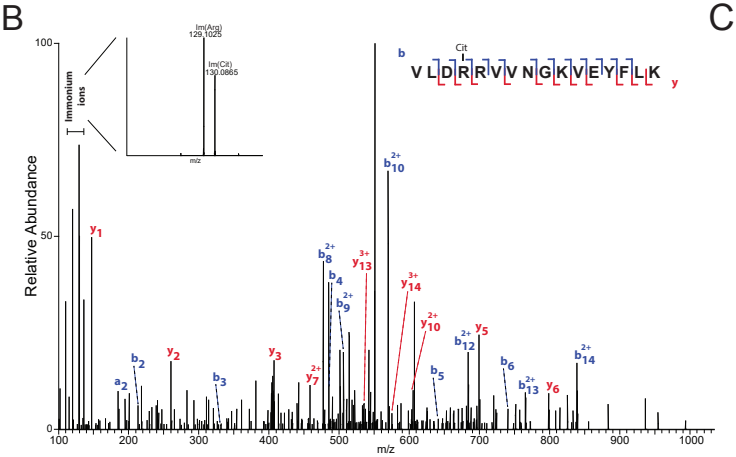
Relative Abundance
m/z
Immonium ions
Im(Arg) 129.1025
Im(Cit) 130.0865
Cit
V L D R R V V N G K V E Y F L K

C

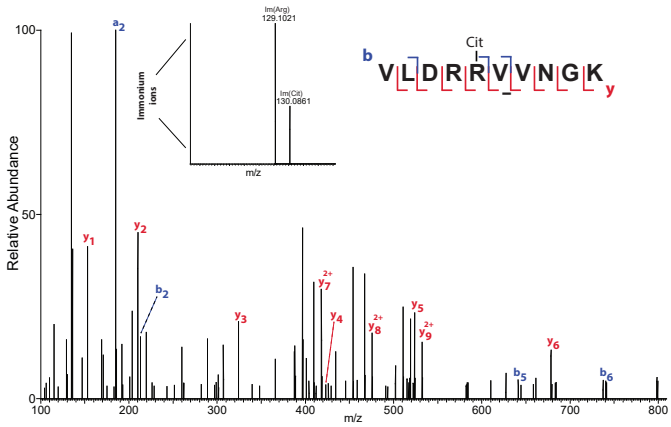
Relative Abundance
m/z
Immonium ions
Im(Arg) 129.1021
Im(Cit) 130.0861
Cit
V L D R R V V N G K

Figure 2

A

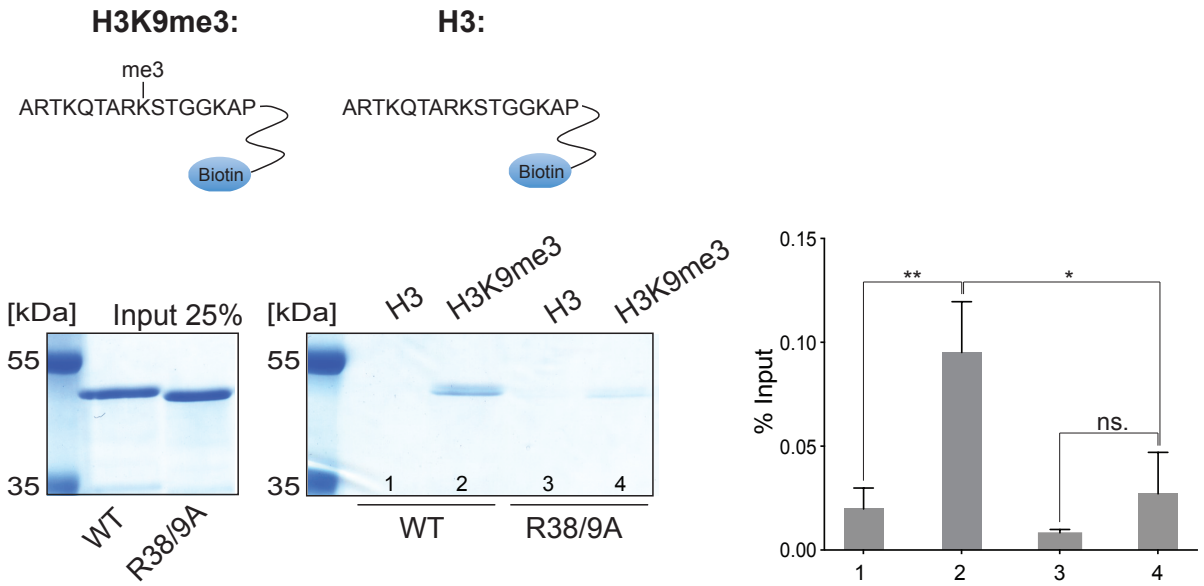
H3K9me3:
me3
ARTKQTARKSTGGKAP
Biotin
H3:
ARTKQTARKSTGGKAP
Biotin
[kDa]
Input 25%
55
35
WT
R38/9A
[kDa]
H3
H3K9me3
H3
H3K9me3
55
35
1
2
3
4
WT
R38/9A
% Input
0.15
0.10
0.05
0.00
**
*
ns.
1
2
3
4

B

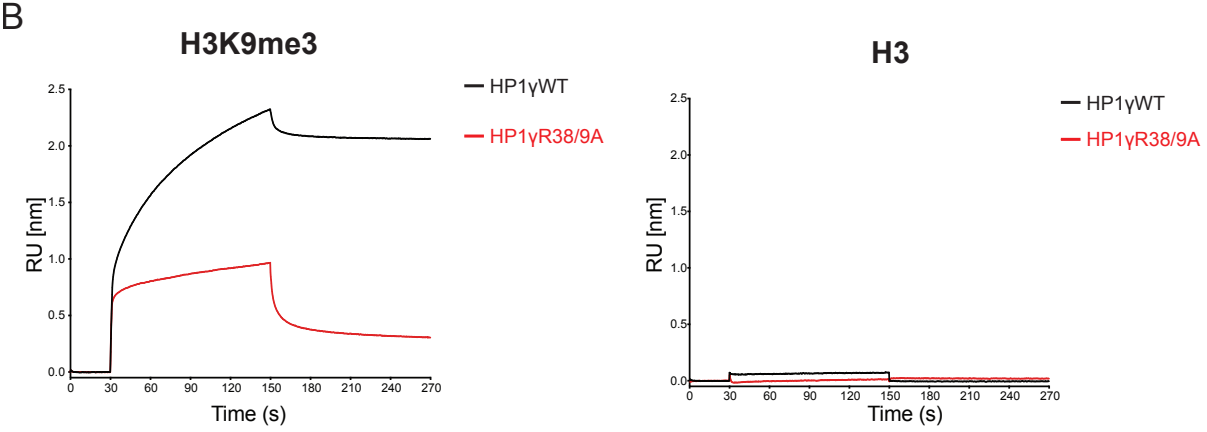
H3K9me3
HP1γWT
HP1γR38/9A
RU [nm]
Time (s)
H3
HP1γWT
HP1γR38/9A
RU [nm]
Time (s)

Figure 3

A

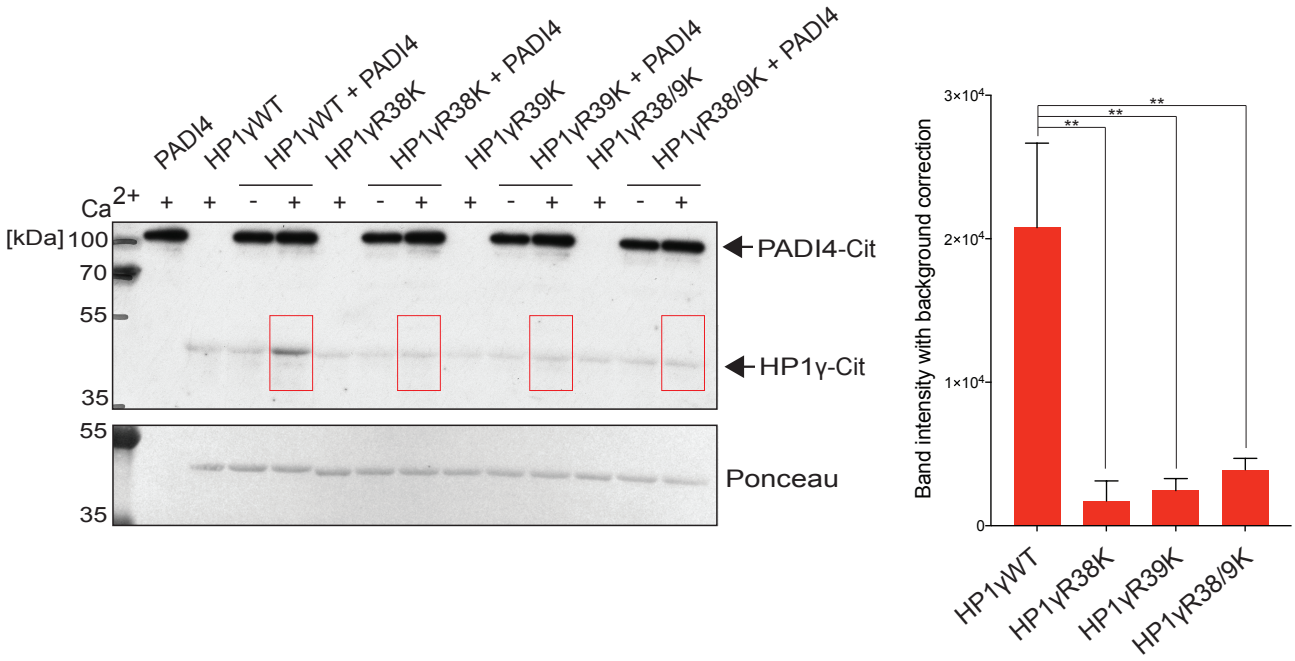
PADI4
HP1γWT
HP1γWT + PADI4
HP1γR38K
HP1γR38K + PADI4
HP1γR39K
HP1γR39K + PADI4
HP1γR38/9K
HP1γR38/9K + PADI4
Ca2+
[kDa]
100
70
55
35
PADI4-Cit
HP1γ-Cit
Ponceau
Band intensity with background correction
3×10⁴
2×10⁴
1×10⁴
0
**
HP1γWT
HP1γR38K
HP1γR39K
HP1γR38/9K

B

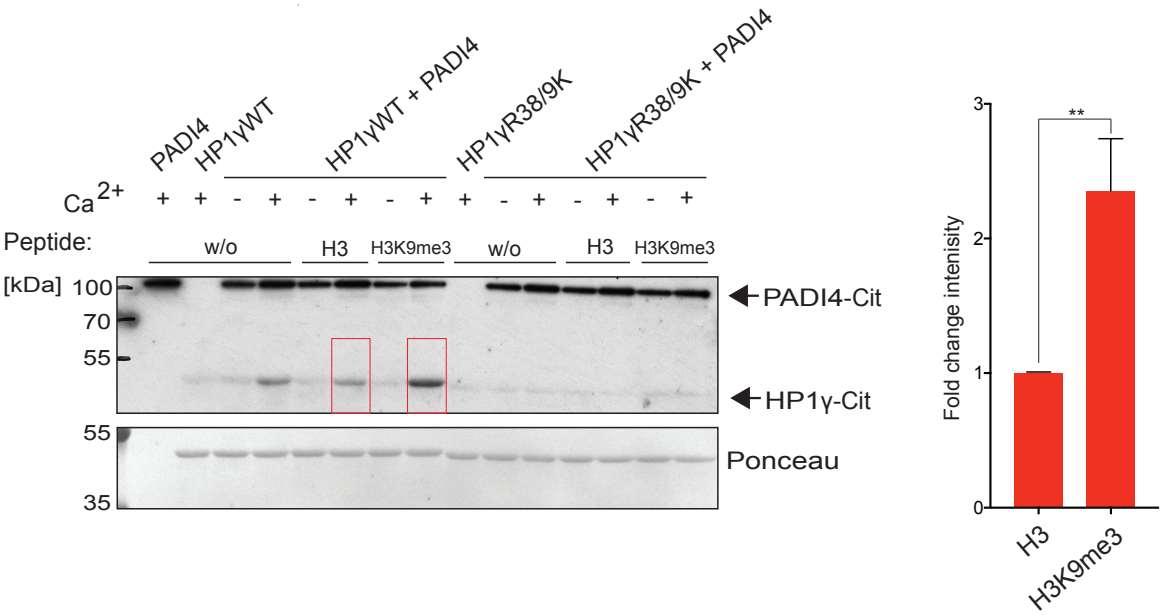
PADI4
HP1γWT
HP1γWT + PADI4
HP1γR38/9K
HP1γR38/9K + PADI4
Ca2+
Peptide:
w/o
H3
H3K9me3
[kDa]
100
70
55
35
PADI4-Cit
HP1γ-Cit
Ponceau
Fold change intenisity
3
2
1
0
**
H3
H3K9me3

Figure 4

A

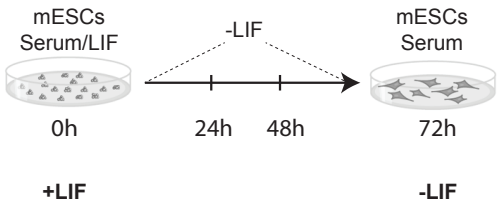

B

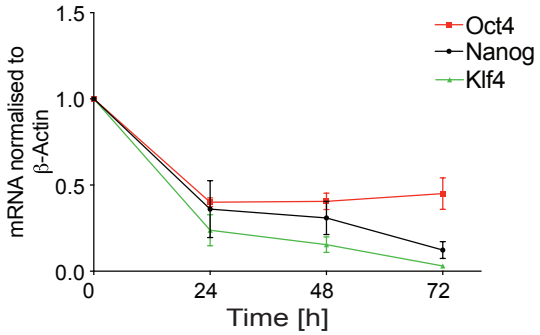

C

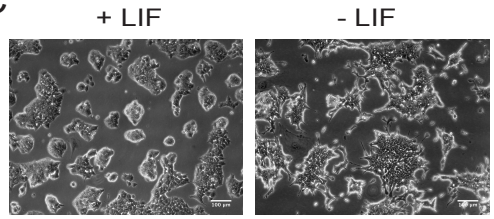

D

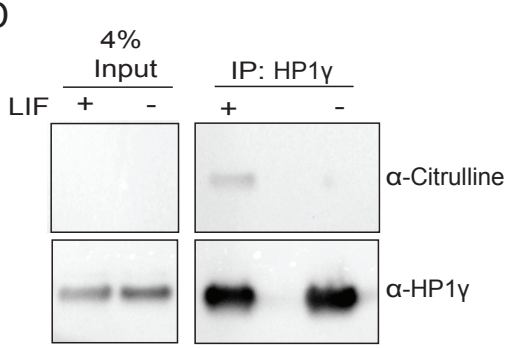

Figure 5

A

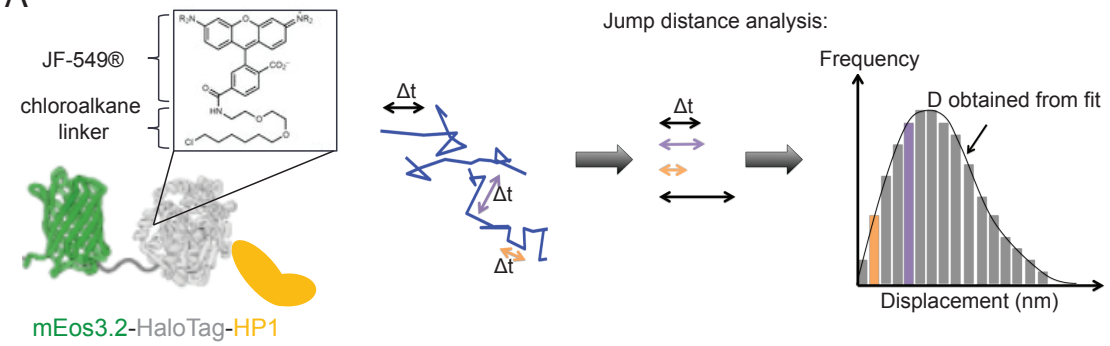

B

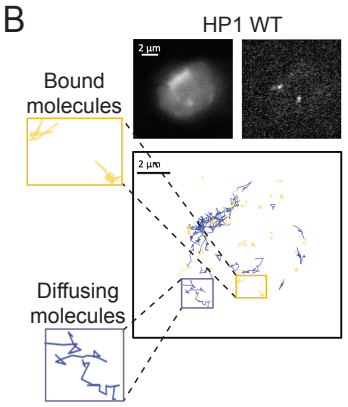

C

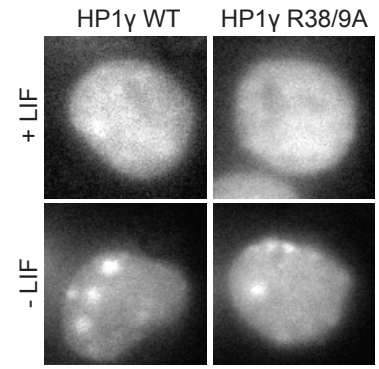

D

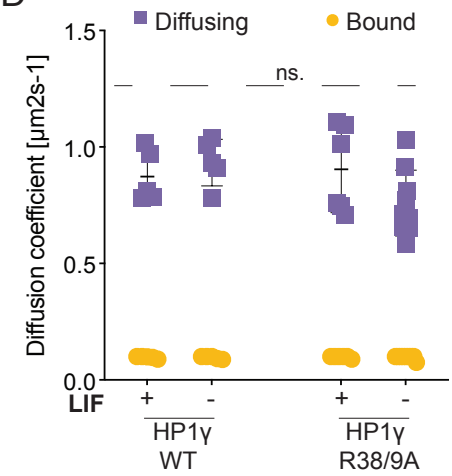

E

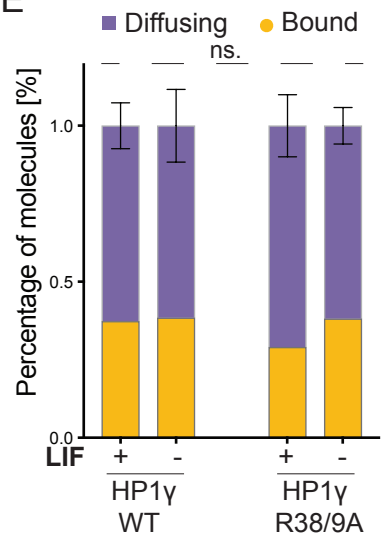

F

		Diffusion coefficient $\mu m^2 s^{-1}$		Percentage %	
		Diffusing	Bound	Diffusing	Bound
+ LIF	HP1γWT	0.87 ± 0.11	0.100 ± 0.004	62.6 ± 7.30	37.4 ± 7.30
	HP1γR38/9A	0.90 ± 0.18	0.100 ± 0.004	70.9 ± 10.0	29.1 ± 10.0
- LIF	HP1γWT	0.92 ± 0.12	0.090 ± 0.007	61.5 ± 11.7	38.5 ± 11.7
	HP1γR38/9A	0.75 ± 0.14	0.100 ± 0.010	63.7 ± 5.80	36.3 ± 5.80

Figure 6

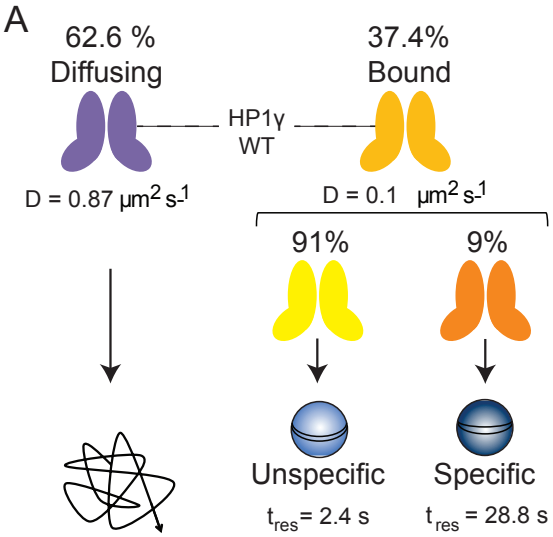

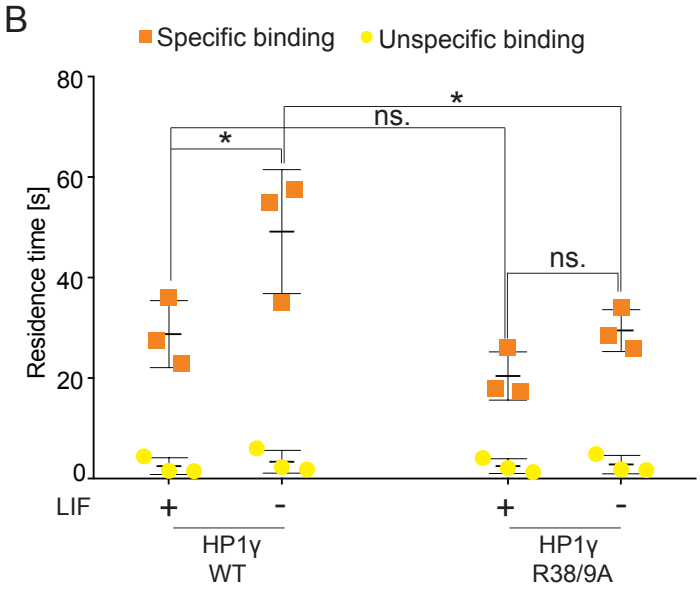

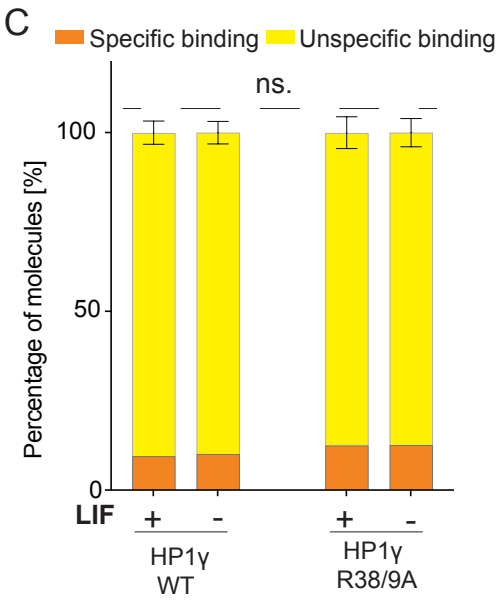

D

		Residence time s		Percentage %	
		Unspecific binding	Specific binding	Unspecific binding	Specific binding
+ LIF	HP1γWT	2.4 ± 1.6	28.8 ± 6.7	90.5 ± 3.2	9.5 ± 3.2
	HP1γR38/9A	2.5 ± 1.4	20.4 ± 4.8	87.5 ± 4.4	12.5 ± 4.4
- LIF	HP1γWT	3.4 ± 2.3	49.2 ± 12.3	89.8 ± 3.2	10.2 ± 3.2
	HP1γR38/9A	2.8 ± 1.8	29.5 ± 4.1	87.3 ± 4.0	12.7 ± 4.0

Figure 7

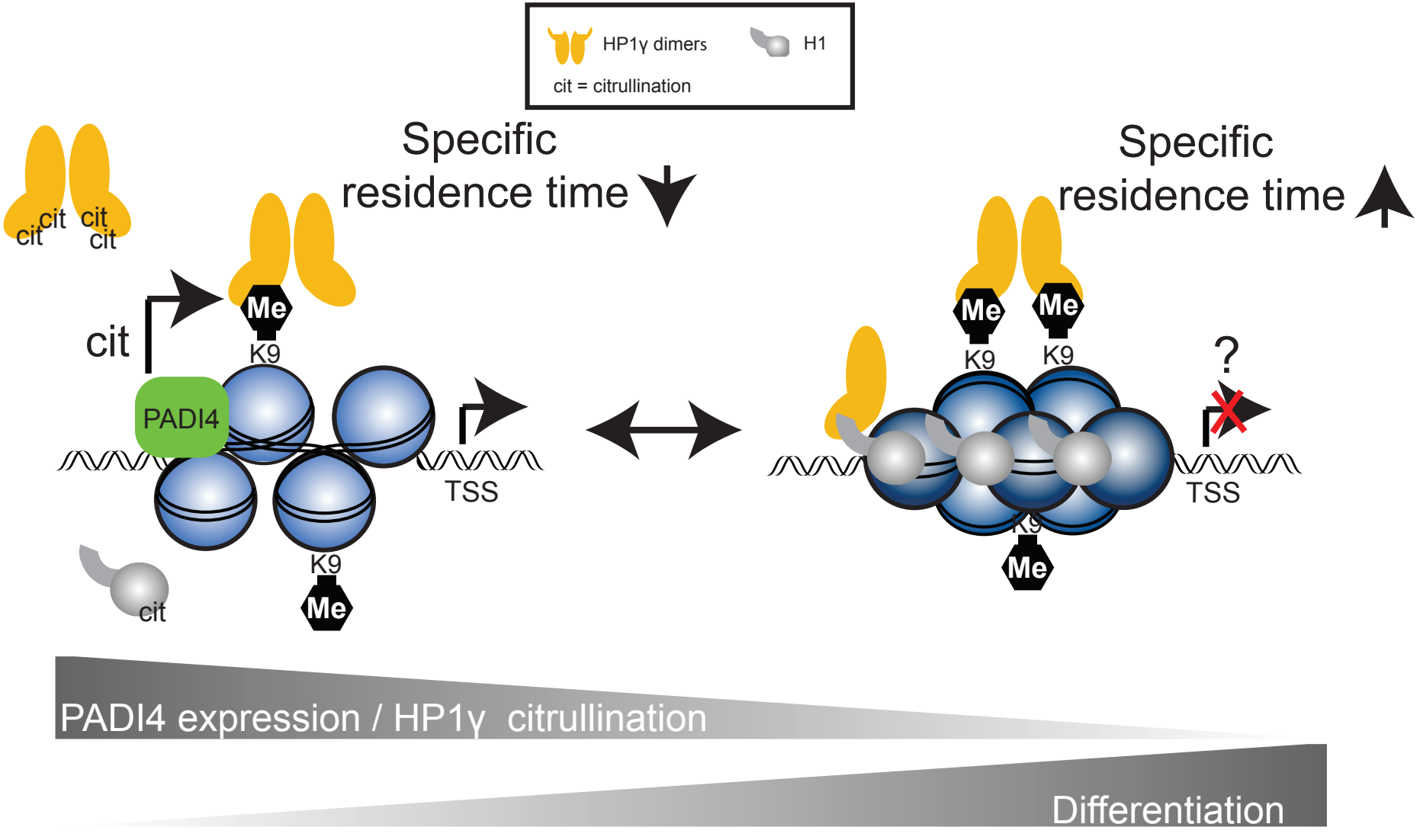
HP1γ dimers
H1
cit = citrullination
Specific residence time
Specific residence time
cit
cit
cit
cit
cit
Me
K9
PADI4
TSS
K9
Me
cit
Me
Me
K9
K9
?
TSS
Me
PADI4 expression / HP1γ citrullination
Differentiation

Citrullination of HP1γ chromodomain affects association to chromatin

Meike Wiese[1,2*], Andrew J. Bannister[1,2], Srinjan Basu[3#], Wayne Boucher[3], Kai Wohlfahrt[3], Maria A. Christophorou[4], Michael L. Nielsen[5], David Klenerman[6], Ernest D. Laue[3], Tony Kouzarides[1,2#]

Additional data:

1. Supplementary Figures 1 - 6

2. Movies 1 - 4

3. Tables 1 - 3

1. Supplementary Figure 1 - 6:

File format: .pdf

Supplementary Figure legends:

Supplementary Figure 1

Citrullination of HP1γ identified by MS/MS

A Multiple sequence alignment of paralogues of mouse HP1 protein sequences using Clustal Omega. Functional domains of HP1 (CD, HR and CSD) and C-terminal and N-terminal extensions are colour-coded as indicated in panel D. Isoleucine residues in the PxVxL motif, known to diminish dimerization of HP1, are highlighted in yellow.

B/C MS/MS fragmentation tables relating to the fragmentation spectra depicted in Fig 1B and C, including the mass accuracies of identified fragments.

D Schematic illustration of HP1γ mutants used in this study. Changes in amino acids are indicated. Functional domains of HP1 are illustrated: CD (blue) is the chromodomain; HR (orange) is the hinge region, and CSD (green) is the chromoshadow domain. C-terminal and N-terminal extensions are indicated in grey.

Supplementary Figure 2

Loss of charge at residues R38 and R39 impairs HP1γ's binding to H3K9me3 in vitro

A Unprocessed images of Coomassie blue stained gels showing the results from pulldown assays analyzing binding of GST-HP1γWT, -HP1γR38/9A, -

HP1γR38/9K, -HP1γR38A and -HP1γR39A mutant proteins to H3K9me3(1-16) or unmethylated H3(1-16) peptides, as indicated. 25% of input amounts are shown. (i) - (iii) show replicates quantified in Fig 2A.

B BLI sensorgrams showing the normalized binding profiles of recombinant GST-HP1γWT, -HP1γR38/9K and -HP1γR38/9A binding to biotinylated H3K9me3(1-16) peptides. On the left sensorgram, association (30-150 s) and dissociation (150-270 s) were each measured over the course of 120 s. Results of one experiment are shown. Protein concentrations used are WT: 28.0 μM; R38/9K: 25.5 μM; R38/9A: 28.3 μM.

C BLI sensorgrams showing the normalized binding profiles of recombinant GST-HP1γWT, -HP1γR38/9K, -HP1γR38/9A and GST binding to biotinylated H3 peptides (H3K9me3(1-16): left panel) or H3(1-16) peptides (H3: right panel). Association (30-150 s) and dissociation (150-270 s) were each measured over the course of 120 s. Results of one experiment are shown. Concentrations used from top to bottom were WT: 28.0 μM, 18.7 μM, 12.4 μM, 8.3 μM, 2.8 μM, 0.9 μM and 0.3 μM; R38/9K: 25.5 μM, 17.0 μM, 11.3 μM, 7.6 μM, 2.5 μM, 0.8 μM and 0.3 μM; R38/9A: 28.3 μM, 18.9 μM, 12.6 μM, 8.4 μM, 2.8 μM, 0.9 μM and 0.3 μM; GST: 30.6 μM, 20.4 μM, 13.6 μM, 9.1 μM and 3.0 μM.

Supplementary Figure 3

PADI4 citrullinates HP1γ in vitro

A/B As a known PADI4 target, recombinant H3.1 was incubated with recombinant PADI4 in the presence of activating calcium. No calcium reactions serve as negative controls. Reactions were resolved by SDS-PAGE

and analyzed by immunoblot analysis using (**A**) an anti-H3R2-citrulline antibody and (**B**) an anti-peptidyl-citrulline antibody.

C Unprocessed images of *in vitro* citrullination assays relating to Fig 3A. GST-HP1γWT, -HP1γR38K, -HP1γR39K or -HP1γR38/9K mutants were treated with GST-PADI4 in the presence or absence of activating calcium, as indicated. Reactions were resolved by SDS-PAGE and analyzed by immunoblot analysis using an anti-peptidyl-citrulline antibody. Images of three biological replicates (i-iii) are shown together with their respective ImageJ quantifications. Quantifications of lanes shown in Fig 3A are highlighted in red.

D Unprocessed images of *in vitro* citrullination assays relating to Fig 3B. GST-HP1γWT or -HP1γR38/9K mutant proteins were treated with GST-PADI4, with or without activating calcium, in the presence or absence of H3(1-16) or H3K9me3(1-16) peptides, as indicated. Images of three replicates (i-iii) are shown together with their respective ImageJ quantifications. Quantifications of lanes shown in Fig 3B are highlighted in red. Images (i-ii) depict autoradiograms whilst image (iii) was acquired using a Chemidoc™ imaging system.

Supplementary Figure 4

Differentiation of mESCs

A Immunoprecipitation (IP) of endogenous HP1γ from nuclear lysates of mESCs before and after 72 h LIF withdrawal. IPs were performed with anti-HP1γ and anti-HA control antibodies and analyzed by immunoblotting using an anti-peptidyl-citrulline antibody (α-Citrulline). Subsequently the same

immunoblots were stripped and re-probed with an anti-HP1γ antibody (α-HP1γ). 4% of input amounts of each IP are indicated. Replicate (i) is shown in Fig 4D.

B Stable exogenous expression of mEos3.2-HaloTag-HP1γ fusion proteins does not affect total mRNA level of pluripotency markers in mESCs. RT-PCR data for the indicated genes was normalized to *β-actin* mRNA expression. Bars represent ± SEM (n=2).

C The mRNA levels of pluripotency markers in mESCs decrease after withdrawal of LIF. The mRNA levels of the indicated genes were measured by RT-PCR over a course of 3 days after withdrawal of LIF. RT-PCR data were normalized to *β-actin* mRNA expression and expression fold-change was determined relative to d_0 time point using the ddCT method. Bars represent ± SEM (n=2).

D Representative lightfield microscope images of mESCs before and after 72 h LIF withdrawal, captured with a Leica EC3 camera at 20x magnification. Scale bars: 100 µm.

<u>Supplementary Figure 5</u>

Single-particle tracking to measure HP1 dynamics in vivo

A Immunoblot analysis of whole cell extracts of mESCs stably expressing or mEos3.2-HaloTag-HP1γWT or fusion proteins. Anti-HP1γ antibody detects endogenous and fusion proteins. β-Tubulin levels are shown as a loading control.

B Representative raw SPT data of mEos3.2-HaloTag-HP1γWT and HP1γI165K molecules in mESCs. Histograms depict fraction of jumps plotted against jump distance [nm] of HaloTag-JF_{549}-tagged HP1 in mESCs.

C Representative jump distance (JD) analyses of mEos3.2-HaloTag-HP1γWT and I165K molecules in mESCs. Cumulative fraction of jumps plotted against JD [μm]. Yellow line indicates the result of fit to JDs of bound molecules ($D \leq 0.1\ \mu m^2 s^{-1}$); orange line shows the result of fit to JDs of diffusing molecules ($D \geq 0.6\ \mu m^2 s^{-1}$); blue line shows result of fit to JDs combining both bound and diffusing molecules and purple line shows the raw data.

D SPT of mEos3.2-HaloTag-HP1γWT and HP1γI165K mutant proteins. Cells were labeled with HaloTag-JF_{549} ligand and subjected to SPT. At 561 nm fluorescent images were collected as movies of 10000 frames at 13.5 ms time resolution. Plot depicts diffusion coefficients (D) [$\mu m^2\ s^{-1}$] of the indicated HP1 molecules. Bars represent ± SD, n=4-5, two-way ANOVA multiple comparisons with Sidak *post hoc* test (****p-value: 0.0001).

E Percentages of molecules within diffusing and bound fraction are shown. Bars represent ± SD (n=4-5), two-way ANOVA multiple comparisons with Sidak *post hoc* test (ns. P-value > 0.165).

F Tabulated summary of results shown in **D** and **E.** Errors represent ± SD (n=4-5).

Supplementary Figure 6

HP1γ R38 and R39 determine chromatin residence time in differentiating mESCs

Bayesian Information Criterion (BIC) of residence time modes. The relative likelihood for each model for each data set was determined by use of the BIC comparing different models for single particle tracking data. The fit with the lowest BIC was used (light blue). Representative results for experiment (i) are shown as a proof of principle. For both HP1γWT and HP1γR38/9A two binding modes were identified as most likely. Parameters describe: t_{res}: residence times; $a_1/(a_1 + a_2)$: percentage molecules binding specifically and unspecifically.

2. Movies 1 - 4

File name: Movie 1

File format: .avi

Title: SPT of mESC expressing HP1γWT cultured in the presence of LIF

Description: Movie of representative mESCs expressing HP1γWT cultured in the presence of LIF of experiment (i) labeled with HaloTag-JF_{549} ligand imaged at 561 nm. Fluorescent images were collected as movies of 1000 frames at 500 ms time resolution.

File name: Movie 2

File format: .avi

Title: SPT of mESC expressing HP1γR38/9A cultured in the presence of LIF

Description: Movie of representative mESCs expressing HP1γR38/9A cultured in the presence of LIF of experiment (i) labeled with HaloTag-JF_{549} ligand imaged at 561 nm. Fluorescent images were collected as movies of 1000 frames at 500 ms time resolution.

File name: Movie 3

File format: .avi

Title: SPT of mESC expressing HP1γWT cultured in the absence of LIF

Description: Movie of representative mESCs expressing HP1γWT cultured in the absence of LIF for 72 h of experiment (i) labeled with HaloTag-JF_{549} ligand imaged at 561 nm. Fluorescent images were collected as movies of 1000 frames at 500 ms time resolution.

File name: Movie 4

File format: .avi

Title: SPT of mESC expressing HP1γR38/9A cultured in the absence of LIF

Description: Movie of representative mESCs expressing HP1γR38/9A cultured in the absence of LIF for 72 h of experiment (i) labeled with HaloTag-JF_{549} ligand imaged at 561 nm. Fluorescent images were collected as movies of 1000 frames at 500 ms time resolution.

3. Tables 1 – 3

File name: Table 1

File format: .xls

Title: Raw BLI data

Description: Raw BLI data of GST, GST-HP1γWT, R38/9A and R38/9K proteins at different concentrations to H3K9me3(1-16) and H3(1-16) unmethylated peptides.

File name: Table 2

File format: .xls

Title: STP data of single replicates

Description: This file contains a summary of all biological replicates of analyzed STP data of mESCs expressing HP1γWT, R38/9A or I165K mutant proteins cultured in presence or absence of LIF for 72 h labeled with HaloTag-JF_{549} ligand imaged at 561 nm at 13.5 and 500ms time resolution.

File name: Table 3

File format: .xls

Title: List of RT-PCR primers used in this study

Supplementary Figure 1

A

```
ms_HP1α ----------MGKKTKR-TADSSSSEDEEEYVVEKVLDRRMVKGQVEYLLKWKGFSEEHN 49
ms_HP1β ----------MGKKQNKKKVEEVLEEEEEEYVVEKVLDRRVVKGKVEYLLKWKGFSDEDN 50
ms_HP1γ MASNKTTLQKMGKKQNGK-SKKVEEAEPEEFVVEKVLDRRVVNGKVEYFLKWKGFTDADN 59

ms_HP1α TWEPEKNLDCPELISEFMKKYKKMKEGENNKPREKSEGNKRKSSFS--NSADDIKSKKKR 107
ms_HP1β TWEPEENLDCPDLIAEFLQSQKTAHET------DKSEGGKRKADSDSEDKGEESKPK-KK 103
ms_HP1γ TWEPEENLDCPELIEDFLNSQKAGKEK------DG---TKRKSLSD--SESDDSKSK-KK 107

ms_HP1α EQSNDIARGFERGLEPEKIIGATDSCGDLMFLMKWKDTDEADLVLAKEANVKCPQIVIAF 167
ms_HP1β KEESEKPRGFARGLEPERIIGATDSSGELMFLMKWKNSDEADLVPAKEANVKCPQVVISF 163
ms_HP1γ RDAADKPRGFARGLDPERIIGATDSSGELMFLMKWKDSDEADLVLAKEANMKCPQIVIAF 167

ms_HP1α YEERLTWHAYPEDAENKEKESAKS 191
ms_HP1β YEERLTWHSYPSEDDDKKDDKN-- 185
ms_HP1γ YEERLTWHSCPEDEAQ-------- 183
```

B

Fragment	Theo. Mass	Exp. Mass	ppm	Fragment	Theo. Mass	Exp. Mass	ppm
y1	147.1134	147.113	-2.72	b1	100.0762		
y2	260.1974	260.1976	0.77	b2	213.1603	213.1604	0.47
y3	407.2658	407.253	-31.43	b3	328.1872	328.1878	1.83
y4	570.3292			b4	485.2724	485.2686	-7.83
y5	699.3718	699.3735	2.43	b5	641.3735		
y6	798.4402	798.4449	5.89	b6	740.4419	740.436	-7.97
y7	926.5351			b7	839.5103		
y8	983.5566	983.5639	7.42	b8	953.5532	953.5553	2.20
y9	1097.5995			b9	1010.5747	1010.5777	2.97
y10	1196.6679	1196.6617	-5.18	b10	1138.6697	1138.6689	-0.70
y11	1295.7364			b11	1237.7381	1237.7329	-4.20
y12	1452.8215	1452.8255	2.75	b12	1366.7807	1366.7835	2.05
y13	1608.9226	1608.921	-0.99	b13	1529.844	1529.8423	-1.11
y14	1723.9495	1723.9553	3.36	b14	1676.9124	1676.913037	0.38
y15	1837.0336			b15	1789.9965		

C

Fragment	Theo. Mass	Exp. Mass	ppm	Fragment	Theo. Mass	Exp. Mass	ppm
y1	153.1335	153.1328085	-4.52	b1	100.0762		
y2	210.1549	210.1547588	-0.67	b2	213.1603	213.1590584	-5.82
y3	324.1979	324.1970257	-2.70	b3	328.1872		
y4	423.2663	423.2618447	-10.53	b4	485.2724		
y5	522.3347	522.3351512	0.86	b5	641.3735	641.371161	-3.65
y6	678.4358	678.4325309	-4.82	b6	740.4419	740.4418113	-0.12
y7	835.5209	835.5169367	-4.74	b7	839.5103		
y8	950.5479	950.5472782	-0.65	b8	953.5532		
y9	1063.6319	1063.632261	0.34	b9	1010.5747		
y10				b10			

D

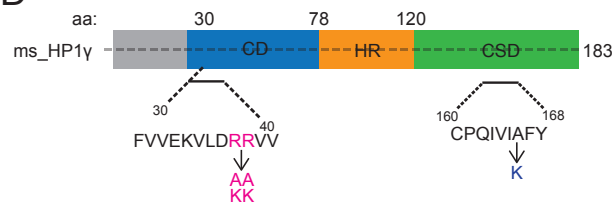

Supplementary Figure 2

A

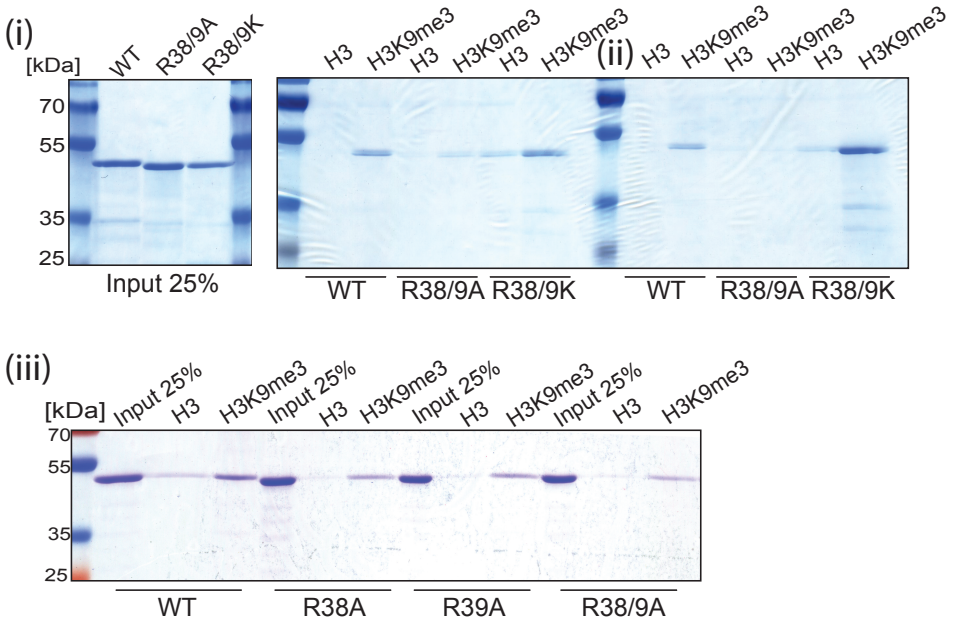

B

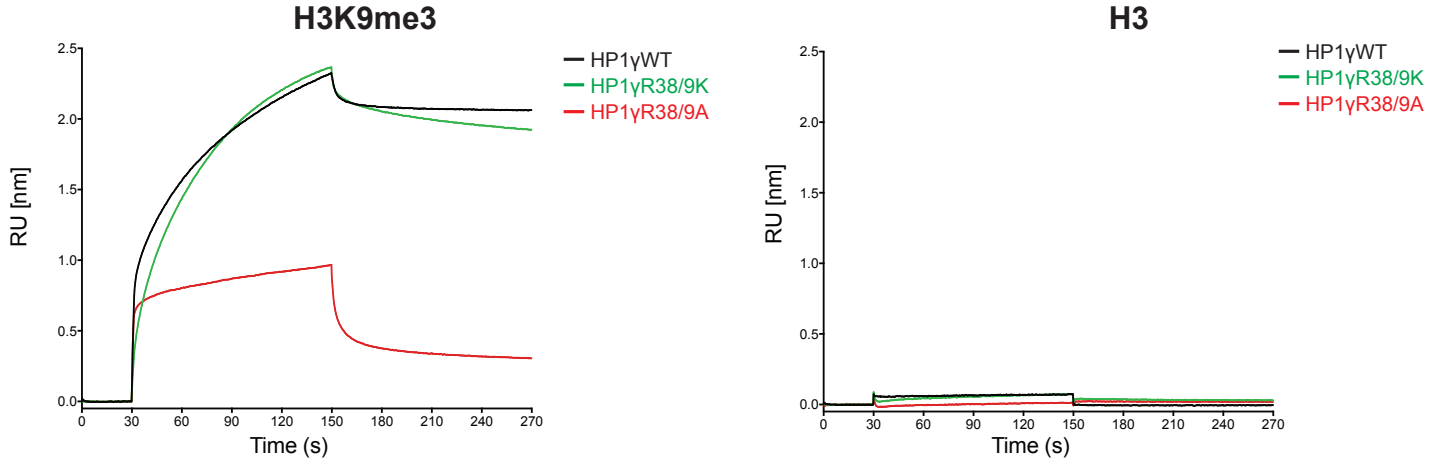

C

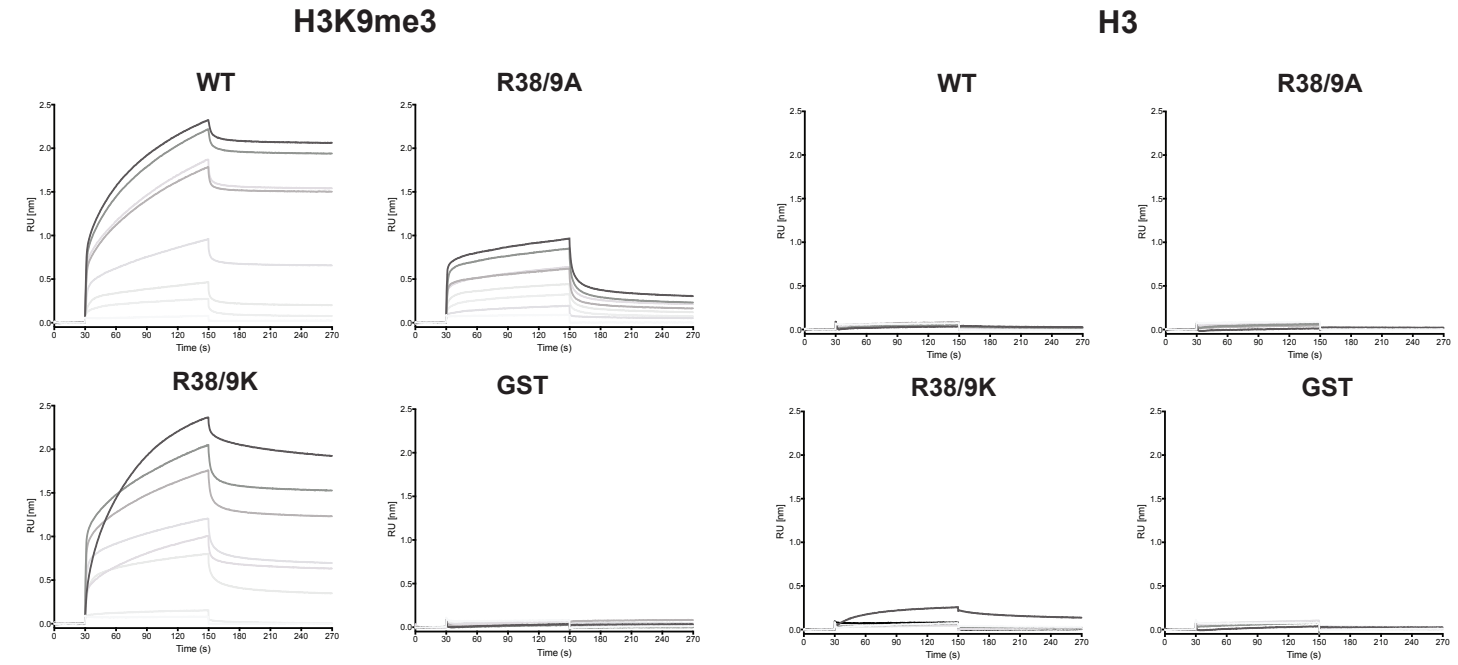

Supplementary Figure 3

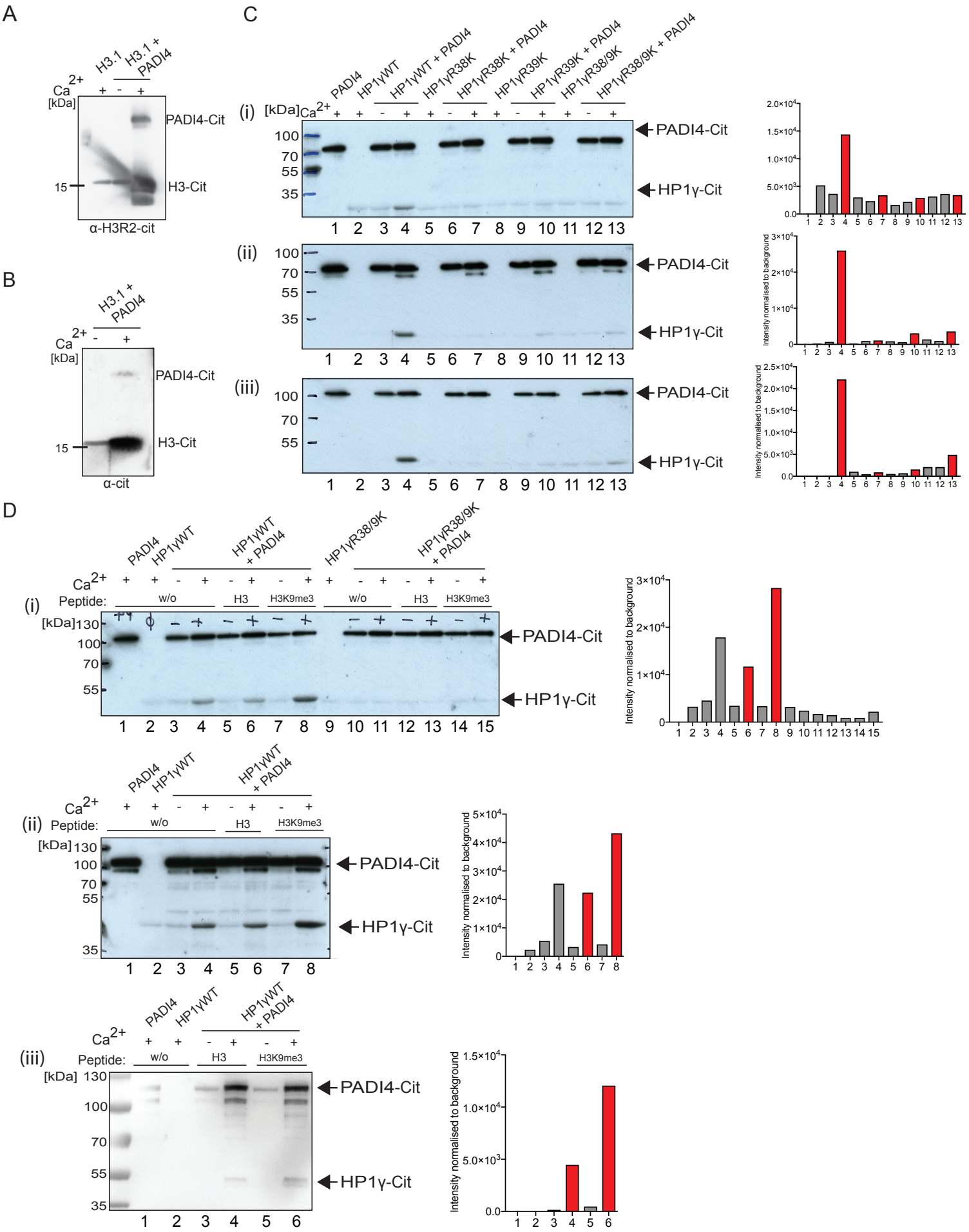

Supplementary Figure 4

A

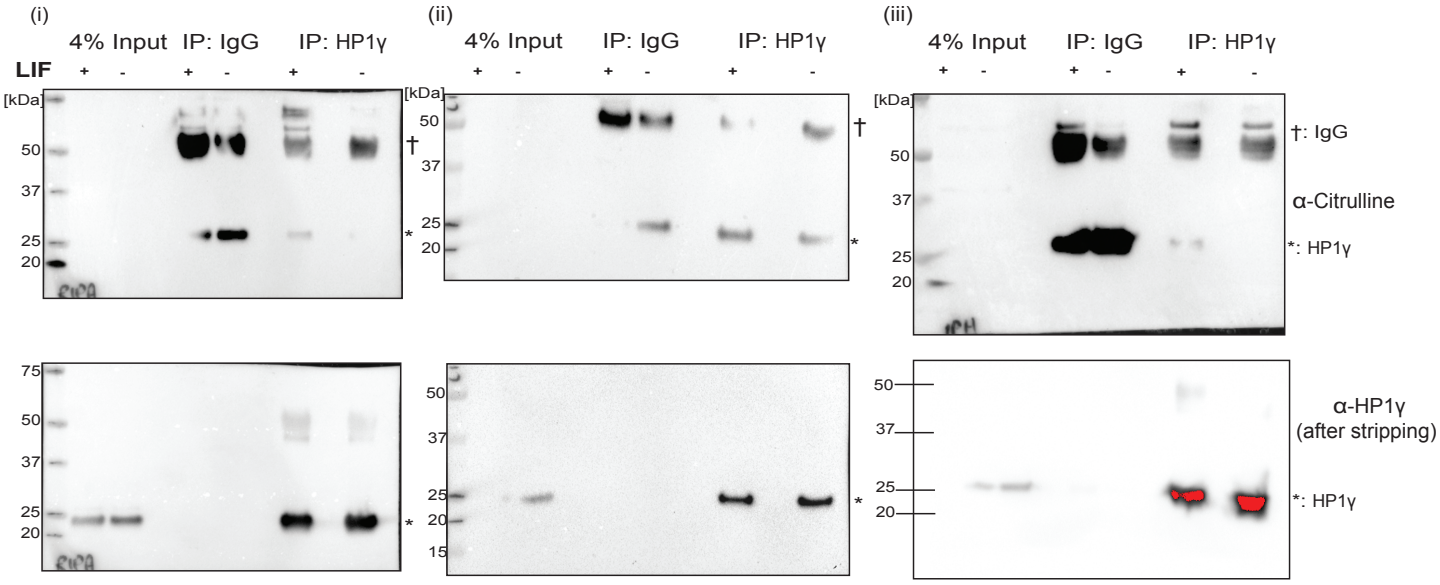

B

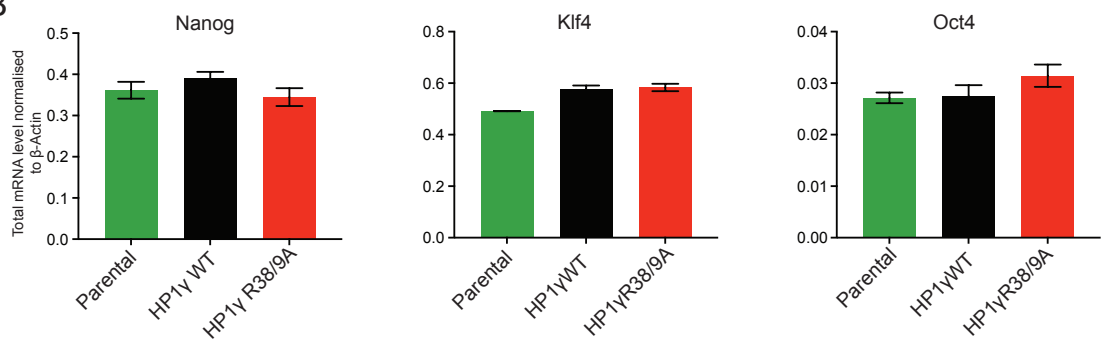

C

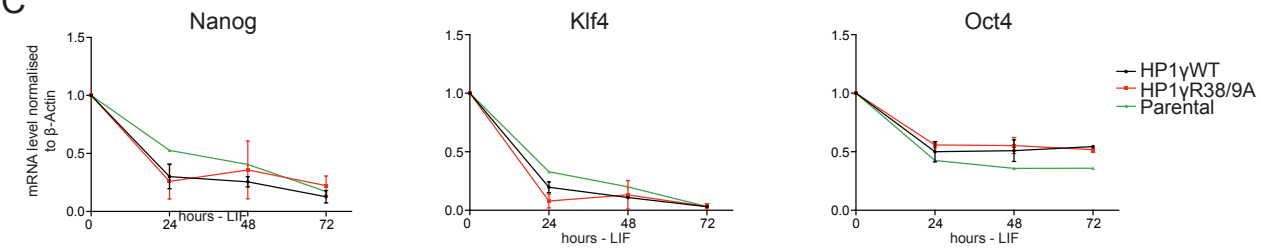

D

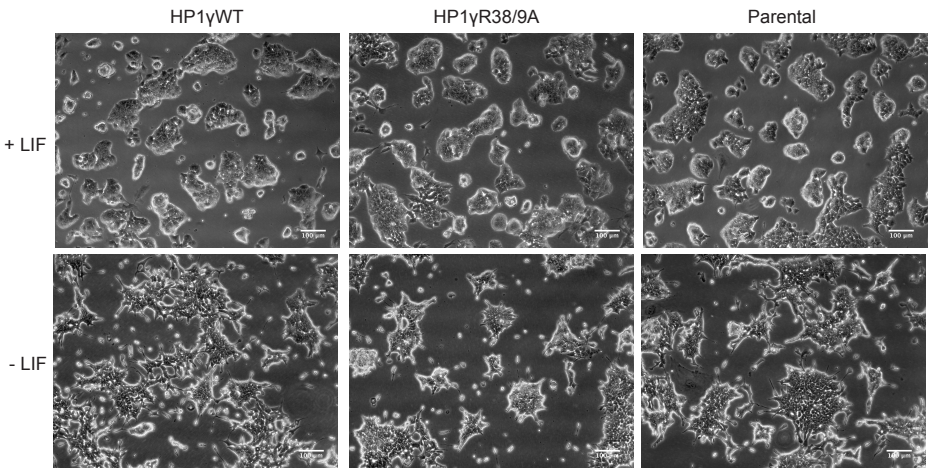

Supplementary Figure 5

A

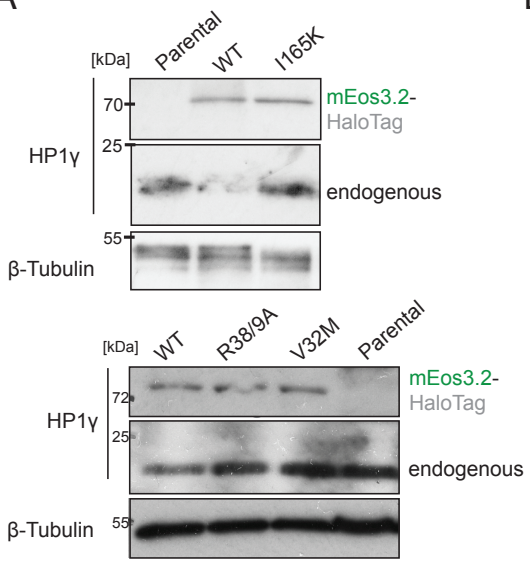

B

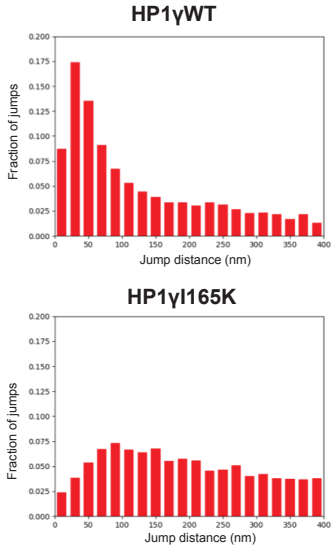

C

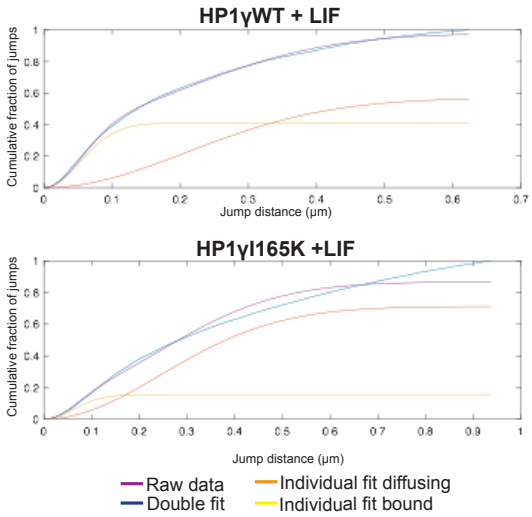

D

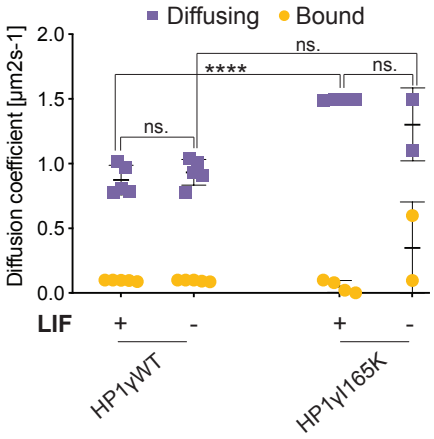

E

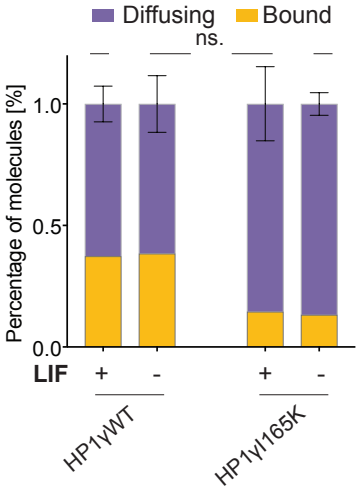

F

	Diffusion coefficient µ m^2s^{-1}		Percentage %	
	Diffusing	Bound	Diffusing	Bound
WT	0.87 ± 0.13	0.100 ± 0.005	62.6 ± 7.3	37.4 ± 7.3
I165K	1.50 ± 0.01	0.05 ± 0.04	85.5 ± 15.1	14.5 ± 15.1

Supplementary Figure 6

	Protein	Bayesian Information Criterion (BIC) $\sum_i a_i \exp(-t/T_i)$			Value $a_1 \exp(-t/T_1)+a_2 \exp(-t/T_2)$			
		i = 1	i = 2	i = 3	$a_1/(a_1+a_2)$	$a_2/(a_1+a_2)$	T_1(s)	T_2(s)
+ LIF	HP1γWT	- 2129.936	-2545.636	-2539.399	0.91 ± 0.02	0.09 ± 0.02	4.4 ± 0.6	36 ± 6
	HP1γR38/9A	- 806.291	-936.202	-927.762	0.89 ± 0.04	0.11 ± 0.04	4.1 ± 0.8	26 ± 6
- LIF	HP1γWT	-1471.080	-2083.957	-2085.414	0.88 ± 0.01	0.12 ± 0.01	6.0 ± 0.22	55.0 ± 4.0
	HP1γR38/9A	-766.59	-1067.488	-1062.498	0.83 ± 0.02	0.17 ± 0.02	4.9 ± 0.11	34.0 ± 4.0